Identifying the optimum storage capacity for a 100-MW_e concentrating solar power plant in South Africa

by

Kamalahasen Madaly

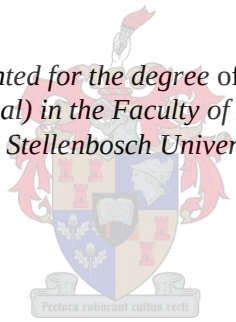

Dissertation presented for the degree of *Master of Engineering (Mechanical) in the Faculty of Engineering at Stellenbosch University*

Supervisor: Dr Jaap Hoffmann
Co-Supervisor: Mr Paul Gauché

April 2014

Declaration

By submitting this thesis electronically, I declare that the entirety of the work contained therein is my own, original work, that I am the sole author thereof (save to the extent explicitly otherwise stated), that reproduction and publication thereof by Stellenbosch University will not infringe any third party rights and that I have not previously in its entirety or in part submitted it for obtaining any qualification.

Signature: .....

Date: .....

Abstract

Central receiver power plants generate renewable electricity by exploiting the energy provided by the sun. The conditions experienced in the Northern Cape region of South Africa provide the ideal conditions for the development of these plants. Without a storage medium these plants have capacity factors in the range of 25-30%. The inclusion of a thermal energy storage medium provides the ability to increase the capacity factors of these plants. Although storage increases the costs, it results in better utilisation of the power block and a decrease in the levelised electricity cost (LEC). Eskom intends building a 100MW_e central receiver dry cooled power plant in the Upington region. This research identifies the appropriate storage medium and ideal storage capacity to achieve the lowest LEC.

A literature survey was performed to identify the different methods of storage that are available. The different storage methods were evaluated and the best storage medium for a central receiver power plant based on the developments of the various storage technologies was identified.

To determine the costs associated with a central receiver power plant, data published by NREL was used. Different plant parameters were required to evaluate the costs. A power plant model based on efficiencies and energy balances was created to determine the required plant parameters. It provided the ability to determine the effect of changing different plant parameters on the LEC and estimate the plant output. The power block parameters were initially varied to determine the most efficient power block configuration. Once the most efficient power block configuration was identified the solar field and storage parameters were varied to determine the plant configuration which resulted in the lowest LEC.

The most efficient power block configuration of 0.4206 was found for a system comprising of six feedwater heaters with the feedwater temperature of 230˚C, main steam pressure 140 bar and an exit steam generator salt temperature of 290˚C. A solar multiple of 3.0 with 16 hours of storage resulted in a LEC of R1.41/kWh with no system constraints. A capacity factor constraint of 60% resulted in a solar multiple of 1.8 with 8 hours of storage and a LEC of R1.78/kWh.

Opsomming

Sonkragaanlegte met sentrale ontvangers wek hernubare elektrisiteit op deur sonenergie te ontgin. Die klimaat in die Noord Kaap-streek van Suid-Afrika is ideaal vir die oprigting van hierdie aanlegte. Sonder ’n bergingsmedium is die kapasiteitsfaktore van sulke aanlegte ongeveer 25-30%. Met die insluiting van ’n bergingsmedium vir termiese energie kan die kapasiteitsfaktore egter verhoog word. Hoewel berging aanlegkoste verhoog, lei dit terselfdertyd tot beter aanwending van die kragblok en ’n afname in die konstante eenheidskoste van elektrisiteit (LEC). Eskom beplan om ’n droogverkoelde kragaanleg van 100 MW met ’n sentrale ontvanger in die Upington-streek op te rig. Hierdie navorsing was dus daarop toegespits om die mees geskikte bergingsmedium en ideale bergingskapasiteit te bepaal om die laagste moontlike LEC uit die aanleg te verkry.

’n Literatuurstudie is onderneem om die verskeie beskikbare bergingsmetodes te bestudeer. Die verskillende metodes is beoordeel, waarna die beste bergingsmedium vir ’n kragaanleg met ’n sentrale ontvanger op grond van die ontwikkelings in die verskillende bergingstegnologieë bepaal is.

Om die koste van ’n kragaanleg met ’n sentrale ontvanger te bepaal, is gepubliseerde data van die Amerikaanse Nasionale Laboratorium vir Hernubare Energie (NREL) gebruik. Verskillende aanlegparameters was egter nodig om die koste te beoordeel. Dié parameters is gevolglik bepaal deur ’n kragaanlegmodel op grond van doeltreffendheidsfaktore en energiebalanse te skep. Sodoende kon vasgestel word watter uitwerking veranderinge in die verskillende parameters op die LEC sou hê, en kon die aanleguitset geraam word. Die kragblokparameters is aanvanklik afgewissel om die doeltreffendste kragbloksamestel te bepaal. Nadat dít bepaal is, is die sonenergieveld en bergingsparameters weer afgewissel om vas te stel watter aanlegsamestel die laagste LEC tot gevolg sou hê.

Die beste termiese benuttingsgraad is behaal vir ’n stoom siklus met ses water verhitters en ’n water temperatuur van 230 °C by die ketel se inlaat, ’n stoom druk van 140 bar, en sout uitlaat temperatuur van 290 °C. ’n Vermenigvuldigingsfaktor van drie vir die heliostaat veld, en 16 uur termiese energie storing gee ’n opwekkingskoste van R 1.41/kW/h indien daar geen beperkings op die grootte of koste van die stelsel geplaas word nie. Indien die kapitaal uitgawe ’n perk van 60 % op die kapasitiet van die stelsel plaas, verander die optimale ontwerpspunt na ’n vermenigvuldigingsfaktor van 1.8, en die termiese stoorkapasitiet verlaag na 8 uur. In hierdie geval is die opwekkingskoste R 1.78/kWh.

Acknowledgements

I would like to express sincere gratitude and thanks to:

- Dr Jaap Hoffmann for his advice and guidance while pursuing this research.
- Paul Gauche for his valuable input, advice and guidance for the solar field modelling and for the project in its entirety.
- Gary de Klerk for always being willing to help, assist and provide guidance and advice when required.
- Prof. Wikus van Niekerk for is advice during the programme.
- Priyesh Gosai for help with the visual basic programming for the parametric analysis.
- Shanley Lutchman for being the sounding board when things just didn't seem to be working out.
- Eskom for accepting me on the Eskom Power Plant Engineering Institute (EPPEI) programme which provided me exposure into the field of renewable energy.
- The EPPEI management team for all their endeavours to ensure success of the programme.
- My line management team of Vernon Fillis, Vernon Paul and Sadika Touffie for supporting me in pursuing this research.

Contents

List of Figures

List of Tables

Nomenclature

A – surface area – m^2

B – day of year in angular value – radians

E – equation of time – minutes

E_t– electricity generation year t – kWh

F_t – fuel expenditures in year t – Rand

h – heat transfer coefficient – W/m^2 K

I_t – investment expenditures in year t – Rand

ITD – initial temperature difference – ˚C

L_{loc} – observer longitude – degrees

L_{st} – longitude of local standard time – degrees

M_t – operation and maintenance expenditures in year t – Rand

$\dot{m}$ – mass flow rate – kg/s

n – life of system - year

n_1 – day of year

$\eta_{optical}$ – optical efficiency of heliostat field – %

$P_{condenser}$ – condenser pressure – bar

P_{sat} – saturation pressure – bar

r – discount rate – %

T_a – ambient temperature – ˚C

T_{db} – dry bulb temperature – ˚C

T_r – receiver temperature – ˚C

V – wind speed – m/s

Greek Symbols

δ – declination

ε – emissivity

η – efficiency

γ_s – solar azimuth angle

α_z – solar altitude angle

θ_z – zenith angle

σ– Stefan Boltzman constant (5.67E – 08)

ϕ – latitude

ω – hour angle (conversion of solar time to an angle where 24hrs is 360 degrees and solar noon is zero)

Abbreviations

avail – availability

CF: capacity factor

CEX: condensate extraction

CSP: concentrating solar power

DSG: direct steam generation

DNI: direct normal irradiation

FWH: feedwater heater

HTF: heat transfer fluid

IRENA: International Renewable Energy Agency

ITD: initial temperature difference

LEC: levelized electricity cost

MW_e: megawatt electric

NREL: National Renewable Energy Laboratory

OCGT: open cycle gas turbine

O&M: operation and maintenance

opt eff: optical efficiency

PV: photovoltaic

refl: reflectivity

sat: saturation

SEGS: Solar Energy Generating Systems

SG: steam generator

SM: solar multiple

S&L: Sargent and Lundy

spill - spillage

TES: thermal energy storage

TMY: typical meteorological year

Definitions

LEC: present price at which the electricity produced must sell so that the net present value associated with the project is zero

Design Point: Point in time and conditions for which the plant is designed to produce its nominal power

Solar Multiple: Ratio of actual solar field size to the minimum size required to run the turbine at full rated capacity at design point

Standard Time: The time that you see on a watch at any location

Capacity Factor: Ratio of actual output of a power plant over a period of time and its output if it had operated at full name plate capacity the entire time. It is measured as a percentage, generally by dividing the total energy produced in a year by the amount of energy it would have produced if it operated at full output over that year

1. INTRODUCTION

1.1 Background

The commercial history of solar thermal power began after the oil crises of the 1970s that prompted many nations to start to investigate renewable energy sources as alternatives to fossil fuels (Cavallaro, 2009). A company called Luz International built a series of parabolic trough plants in California's Mojave Desert. These plants utilised oil as the heat transfer fluid, and this was used to convert water into steam to generate electricity using a conventional steam turbine.

Once the price of natural gas fell and the tax incentives by the American government were not renewed, the interest in solar thermal power gradually disappeared as it was not financially viable.

The acceptance that fossil fuels are limited and the oil shock that has been experienced in recent years have led to a constant increase in fuel costs. This, coupled with acceptance that the increased rate of global warming as a result of using fossil resources is a serious threat, results in greater interest being focussed on electricity generation from renewable resources, in particular solar thermal power.

A problem that is experienced with solar thermal power when used for electricity generation is that power cannot be generated when there is inclement weather or when the sun is not shining (at night). This can be overcome by utilising a thermal energy storage (TES) system. This research focused on identifying and optimising the storage capacity of the ideal TES material for a $100MW_e$ concentrating solar power (CSP) central receiver plant based in South Africa.

1.2 Concentrating solar power

A key factor in exploiting the energy provided by the sun is the use of CSP technology. Mirrors are used to concentrate solar radiation to a central point. This energy is used to heat a fluid that is used to either power a turbine-generator set or to heat a thermal storage medium that allows stored energy to be utilised at a later stage. Figure 1 shows the operating principle of a CSP central receiver plant.

The most favourable CSP technology for the future is the central receiver/power tower technology as it has the promise to reach higher temperatures than the other available CSP technologies. The power tower consists of multiple mirrors called heliostats that reflect the solar radiation to a central point (receiver) to heat a heat transfer fluid (HTF) that in turn is used to heat the electrical generation plant

working fluid to generate electricity. When this system is coupled with a thermal energy storage (TES) medium, it has the ability to produce base load or dispatchable power.

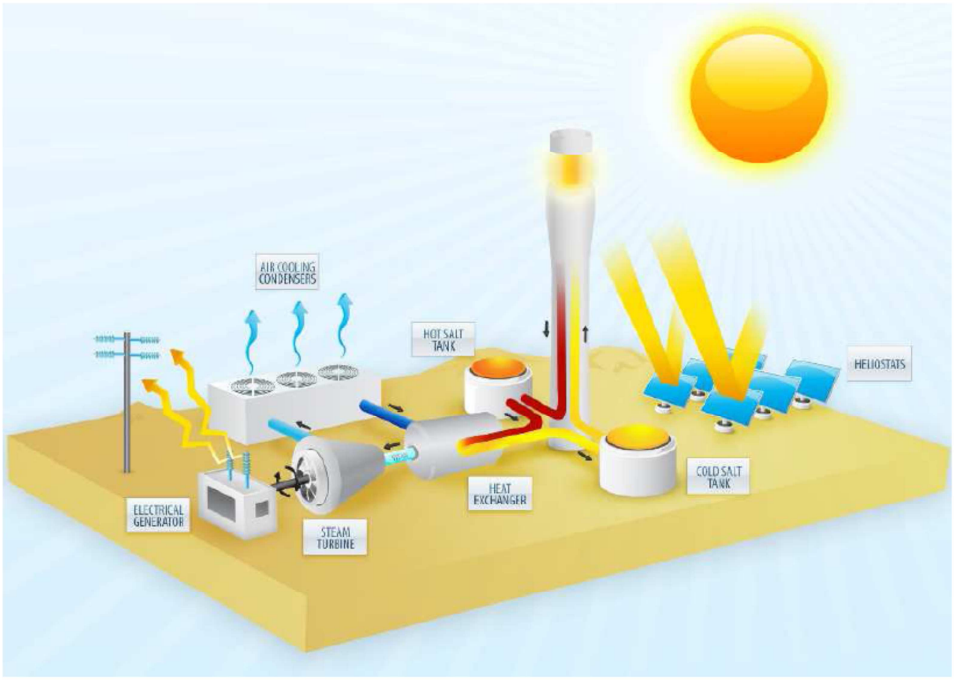

Figure 1: CSP tower plant with two-tank molten salt storage

Source: Dunn, 2010.

The Gemasolar power plant, which is 19.9 MW_e with 15 hours of storage capacity, was commissioned in 2011 in Spain. It is the first commercial molten salt central receiver plant to be commissioned and demonstrates the technology. Assuming a base direct normal irradiation (DNI) of 2 100 kWh/m^2/yr (typical for Spain), the expected levelised electricity cost (LEC) of a CSP plant is expected to decline by 4.5% for every 100 kWh/m^2/yr that the DNI exceeds 2 100 kWh/m^2/yr (International Renewable Energy Agency, 2012b). The semi-arid conditions in the Northern Cape region of South Africa provide the ideal conditions to exploit the potential that central receiver technology has to offer. Eskom thus intends building a 100-MW_e demonstration plant in Upington with TES included.

1.3 Objective of research

The inclusion of storage increases the capital cost of the plant but results in a decreased LEC as there is better utilisation of the power block. The resultant

limited number of stop-start cycles would prolong the turbine life. The objective of this research was to identify through a literature survey the storage technology that should be used for a 100MW_e CSP plant located in Upington South Africa. The power block setup that provides the highest efficiency for a 100MW_e CSP plan was then identified and the storage capacity and solar multiple that provided the minimum LEC was determined using cost data from NREL. This was identified for an unconstrained situation and for a 60% capacity factor constraint.

1.4 Limitations of research

CSP receiver plants are in their infancy in the power generation environment. A 100-MW_e CSP receiver plant has to date not been commissioned, and as such no actual costing data are available to compare against. Several plants are currently under construction or being planned, and this is shown in Appendix A. As the industry is still in the development phase, limited credible sources to determine costing for a plant are available. The most credible information published is that by National Renewable Energy Laboratories (NREL) and the International Renewable Energy Agency (IRENA). The NREL data, published in 2003, were based on a study performed by the Sargent and Lundy LLC Consulting Group, which provided estimates by Sunlab and Sargent and Lundy. The data published by IRENA are estimates based on developments since 2003.

There is major potential for localisation of components in South Africa. This would greatly influence the costing of components. Due to the age of the referenced data and the uncertainty surrounding localisation, it is expected that the values obtained from the referenced sources could be lower than commercial values as they are optimistic values based on expected future scenarios.

1.5 Report outline

This report comprises the following sections:

Chapter 1 provided an introduction to the context of CSP plants and sets out the objectives and limitations for this research. This is followed by a literature survey of the different types of storage material available in Chapter 2.

Chapter 3 identifies a suitable storage material for a central receiver plant and describes the components of a CSP receiver plant.

In Chapter 4 information with respect to the costs involved in central receiver plants is presented. The modelling performed for this research is then explained in Chapter 5, and the validation of the model is covered in Chapter 6.

Chapter 7 covers the parametric analysis performed and presents these results with a discussion.

The report is concluded in Chapter 8, and Chapter 9 provides recommendations for future research. This is followed by the references and appendices.

2. LITERATURE REVIEW

2.1 Renewable technologies

Renewable technologies available for generation of electricity include CSP systems, solar photovoltaic (PV) systems and wind turbines. A solar PV system is an electronic device that converts sunlight directly into electricity (International Renewable Energy Agency, 2012c). Wind power technologies transform the kinetic energy of the wind into useful mechanical power (International Renewable Energy Agency, 2012d). CSP systems without storage, solar PV systems and wind energy are all intermittent sources of power generation. CSP systems without storage and solar PV systems are unable to produce power when there is inclement weather or at time when the sun is not shining. At times when there is no wind, wind turbines are unable to operate.

The capacity factor of a CSP plant without storage is approximately 25% while a solar PV plant experiences capacity factors in the range of 11–23%, dependent on location (International Energy Agency, 2010). Wind power capacity factors are in the range of 20–40% (Wind Energy Centre, University of Massachusetts Amherst, s.a).

Including TES in a CSP plant is an attractive option as it enables the capacity factor to be increased to approximately 80% (International Renewable Energy Agency, 2012b). It also enables the plant to dispatch power when required, and this sets CSP systems with storage apart from other renewable technologies. It is for these reasons that CSP systems with storage are a better option to investigate for areas with appropriate environmental conditions.

2.2 Thermal energy storage

CSP plants with storage have similar or lower LEC than those without. Daily during times of high solar insolation, energy is stored, and during times of limited solar insolation, energy is extracted from storage and used to produce electricity. TES can raise the capacity factor for a given plant and allows for a flexible generation strategy that provides the ability to maximise the value of the electricity generated.

Three storage methods have been considered for the storage of solar thermal energy, namely sensible, latent energy and thermochemical energy. It must be noted though that only sensible heat storage has actually been used in real solar power plants, although both latent and thermochemical storage offer some advantages and are the target storage technologies for future plants (Gil et al., 2009).

2.2.1 Sensible heat storage

Sensible heat storage is the storage of thermal energy in a substance that experiences a change in internal energy, which results in a temperature change in the substance (Gil et al., 2009). No phase change is experienced in sensible heat storage. The density, specific heat, operational temperatures, thermal conductivity, diffusivity and vapour pressure are considered when identifying a suitable material for sensible heat storage (Gil et al., 2009). The density, specific heat and operational temperature limits influence the storage volume of the substance required. The material must have good thermal conductivity and be inexpensive to be useful as a TES medium. An increase in vapour pressure would result in pressurised facilities being required for storage, which would increase storage costs.

Two types of sensible heat storage exist, namely direct and indirect storage. For a direct storage system, the medium used for storage is also used as the HTF. In an indirect storage system, different mediums are used as the HTF and for storage. A heat exchanger exists between the HTF and the storage material to allow for transfer of the thermal energy from the HTF to the storage material and vice versa. The indirect storage system is utilised for parabolic trough power plants.

2.2.1.1 Indirect storage

The indirect storage system was used at the Andasol-1 plant. Oil was heated to 393 ˚C by the parabolic trough field. Some of this oil was fed to the oil-to-steam heat exchanger, which enabled immediate power production. The remaining oil was passed through the oil-to-salt heat exchanger to heat molten salt that was stored in a tank at 386 ˚C. When required for power production, the molten salt is used to heat the oil, which is used to produce steam to generate electricity (Dunn, 2010).

2.2.1.2 Direct storage using oil

This type of storage system was utilised in the Solar Energy Generating System 1 (SEGS 1) power plant in California. Mineral oil called Caloria that was specifically designed for this application was used as the HTF and storage material. The oil was stored in two different tanks; the hot tank after being heated by the solar field was at a temperature of 307 ˚C, and the cold tank after discharging its energy to the power block was at 240 ˚C. As power plants moved to higher operating temperatures to increase power cycle efficiency, there was a switch to higher temperature HTF. Caloria has a high vapour pressure, and

pressurised tanks are very expensive and cannot be manufactured in large sizes. Therefore, the storage concept of SEGS 1 was not repeated in later SEGS plants (Medrano et al., 2009). This temperature is not suitable for use in CSP tower systems.

2.2.1.3 Two-tank molten salt system

The two-tank molten salt system was demonstrated at the Solar Two facility near Barstow, California. Molten salt that was comprised of 60% sodium nitrate and 40% potassium nitrate (Tyner et al., s.a) was used as the HTF and also as the storage medium. The use of fluid with this dual function avoids having to fit out the system with costly heat exchangers and therefore would allow for a substantial reduction in the overall cost of thermal storage (Cavallaro, 2009). The hot and cold molten salts are stored in separate tanks. The molten salts, which have a lower operating limit of 220 ˚C and an upper operating limit of 600 ˚C (Kearney et al., 2002), generate temperatures that allow the Rankine steam cycle turbines to operate at a high efficiency. A disadvantage is that the molten salts solidify at high temperatures (between 120 ˚C and 221 ˚C). This requires the use of trace heating to maintain the salts in a liquid state in the pipes even when the solar radiation is insufficient to do so (Cavallaro, 2009). Molten salts are chosen because they provide an efficient heat storage system; they are nontoxic, eco compatible and cheap (Cavallaro, 2009). The primary advantages of molten salts as the HTF for a power tower are a lower operating pressure and better heat transfer (and thus higher allowable incident heat flux) than a water/steam receiver (Tyner et al., s.a).

Figure 2 shows a schematic of Solar Tres (Gemasolar). It is the first commercial central receiver power plant commissioned. It utilises a combination of the Solar One and Solar Two technology to achieve commercial electricity production of 19.9 MW_e. The thermal storage system is based on the two-tank direct technology, which implies that the fluid used as the storage medium is the same as the HTF. The plant was designed with 15 hours of storage capacity (Medrano et al., 2009).

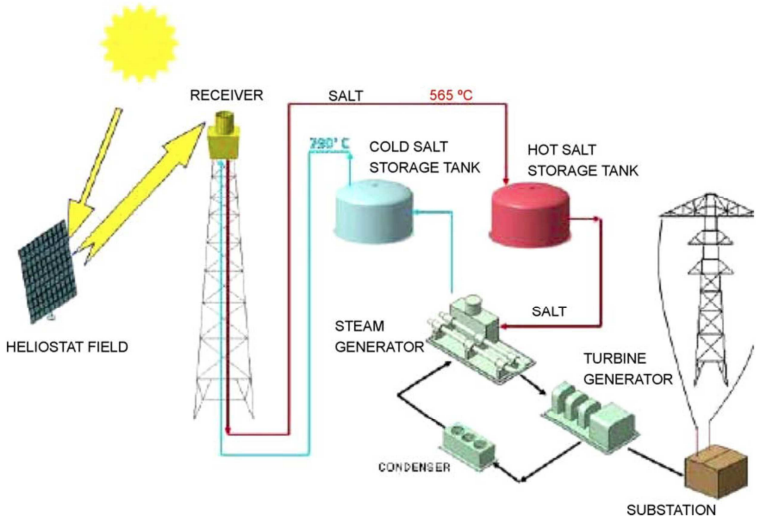

Figure 2: Schematic of Solar Tres (Gemasolar)

Source: Medrano et al., 2009.

2.2.1.4 Thermocline storage

The thermocline system uses a single tank with the hot and cold fluids being stored in the same tank. The hot and cold fluids are separated as a result of stratification. The zone between the hot and cold fluids is called the thermocline. In the thermocline system, the hot fluid is at the top and the cold fluid is at the bottom. The HTF from the solar field passes through a heat exchanger, heating the thermal storage medium that is stored in a single tank. To reduce the inventory of the HTF, a low-cost filler material is utilised. Experimental studies show that the filler material acts as the primary storage medium. The thermocline storage system has the potential to result in a substantially lower cost storage system. An advantage of this system is that most of the storage fluid can be replaced with a low-cost filler material such as quartzite rock (Gil et al., 2009). Disadvantages of the thermocline system are that maintaining the thermal stratification requires a controlled charging and discharging procedure, and appropriate methods or devices to avoid mixing. Design of the storage system is complex, and thermodynamically it is an inefficient power plant (Gil et al., 2009). Thermal ratcheting is another major problem that needs to be overcome before this technology can be realised. In power tower use, thermal ratcheting is exacerbated since there is a higher temperature differential between the top and bottom of the tank (Kolb et al., 2011). Thermoclines have more complex operating requirements

than the two-tank molten salt system, which creates the potential for utilisation and performance losses (Hermann et al., 2002).

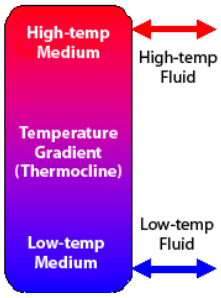

Figure 3: Single-tank thermocline energy storage system

Source: Concentrating solar power thermal storage system basics, 2013.

2.2.1.5 High-pressure steam for direct steam generation

High-pressure steam is used for direct generation of steam. Temperatures of up to 400 ˚C and 100 bar are achieved. The advantage of direct steam generation (DSG) is that the steam turbine can be directly supplied without the need to resort to a heat exchanger, as required when using mineral oils or molten salts (Cavallaro, 2009).

CIEMAT and the DLR are testing DSG at Plataforma Solar de Almeria in Spain. Although there are a number of technical issues that need to be addressed, DSG is still one of the most promising opportunities for future cost reduction. Fast reaction times and high discharge rates with a thermal capacity in the range of 5–10 minutes (Steinmann et al., 2006) make steam accumulators one of the best options for compensation of fast transients in insolation for solar thermal systems using steam as working medium (Medrano et al., 2009).

2.2.1.6 Solid storage media

Storage of thermal energy using high-temperature concrete was demonstrated for a parabolic trough system. In solid storage media, the heat transfer medium passes through the system only for charging/discharging of the system. A pilot plant designed for this application is found at Plataforma Solar de Almeria where a tubular heat exchanger is integrated into the storage material, which is high-temperature concrete. It has a storage capacity of approximately 350 kWh and operates at a maximum temperature of 390 ˚C (Cavallaro, 2009). The temperatures developed by this application are not suitable for tower plants as

they operate at a higher temperature range. The advantages of concrete systems are very low cost of TES media, high heat transfer rates into and out of the solid medium (due to good contact between the concrete and piping), facility of handling of the material and low degradation of heat transfer between the heat exchanger and the storage material. The disadvantages are increase in cost of heat exchanger and of engineering and long-term instability (Gil et al., 2009).

2.2.2 Latent heat storage

Thermal energy can be stored nearly isothermally in some substances as the latent heat of phase change, as heat of fusion (solid-liquid transition) or as heat of vaporisation (liquid-vapour transition). Presently, mainly the solid-liquid transition is used, and substances used under this technology are referred to as phase change materials (PCM) (Gil et al., 2009). Liquid-gas transition requires a large volume recipient for the PCM (Fernandes et al., 2012).

Compared to sensible heat storage, latent heat storage allows large amounts of energy to be stored in relatively small volumes, resulting in some of the lowest storage media costs of any storage concepts (Gil et al., 2009). The low thermal conductivity of PCM, which results in slow charge-discharge rates, is a major disadvantage as it limits the application of latent heat storage technology in practical systems (Barlev et al., 2011; Liu et al., 2012). It is suggested that PCM composite materials be fabricated to alleviate this problem (Barlev et al., 2011).

The thermal, physical and chemical properties of materials are used to determine whether the material will be suitable for latent heat storage. The thermal properties required are phase change temperature within the desired operating range, high latent heat-per-unit mass, high specific heat and high thermal conductivity for both solid and liquid phases. Physical properties are high energy density, low-density variation during phase change and no supercooling during freezing. Chemically it is required that there is chemical stability, there is no chemical decomposition and there is compatibility with container materials construction (vessels and piping), and the material should be nontoxic, nonflammable and nonexplosive. The material should be inexpensive and available in large quantities to be suitable to be used for latent heat storage (Fernandes et al., 2012).

At the DLR (German Aerospace Centre), latent heat systems are currently developed for industrial process heat (temperature range 100–300 ˚C) and solar thermal power plants with DSG (temperature range 300–400 ˚C). The materials being investigated for latent heat storage are salt/graphite composite materials (Tamme et al., 2006).

The TES system shown in Figure 4 consists of a bundle of 36 parallel tubes comprises of six pipes arranged in six passes with fins; the conductive fins are

made of expanded graphite foil, spaced 10 mm apart and perpendicular to the pipes, and have a section of 490 x 490 mm^2 and a thickness of 1 mm (Oro et al., 2012).

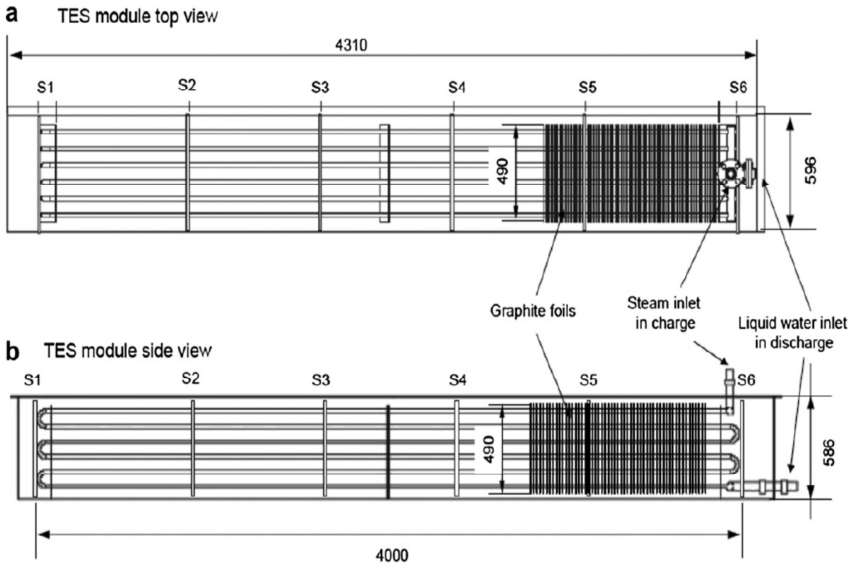

Figure 4: Top and side view of a PCM prototype module

Source: Oro et al., 2012.

At Stellenbosch University, research is being conducted into the use of a eutectic aluminium silicon alloy, AlSi12, as a potential PCM with NaK as the HTF. NaK is a eutectic alloy of sodium (22%) and potassium (78%). Due to the high reactivity of NaK, the proposed concept separates the NaK from steam or water. The NaK is heated up by pumping it through a primary heat transfer loop. It is then pumped through thermal storage tanks that contain stainless heat transfer bundles. In the storage tanks, the thermal energy is transferred to the AlSi12 at 577 ˚C. The ALSi12 is at its melting temperature, and the heat transferred to it from the NaK increases the saturation of the melt. The ALSi12 melt is cooled down by the steam water pipes running through the storage tanks. Superheated steam is generated by cooling the AlSi12, and this is used to drive the turbines (Kotze et al., 2013).

2.2.3 Thermochemical storage

Thermochemical storage is the use of chemical reactions to store the thermal energy generated at the solar receiver. Completely reversible chemical reactions are required for this method to be feasible. The heat produced by the solar

receiver is used to excite an endothermic chemical reaction. As long as this reaction is completely reversible, the thermal energy can be recovered completely by the reverse reaction (Gil et al., 2009). Solar thermal technologies via thermochemical conversion paths offer the prospect of systems with inherent energy storage for continuous (24-hr) generation of electricity (Gil et al., 2009). Development of this technology is at a very early stage, and to date no viable prototype plant has been built (Glatzmaier, 2011). Ammonia, hydroxide, carbonate, hydride and sulphate reactions have been investigated in the past (Gil et al., 2010; Romero-Paredes et al., 2006). These storage systems require the storing of gases at high pressure as they are formed during the endothermic reaction. These gases are required to be stored to enable the exothermic reaction that releases heat to be performed (Romero-Parades et al., 2006). There are studies that claim that ammonia and the SnOx/Sn reactions might be the most suitable ones, but further investigation is still required (Gil et al., 2009). The advantages of thermochemical storage are high storage densities and infinitely long storage duration near ambient temperature (Gil et al., 2009; Glatzmaier, 2011). The disadvantages are complexity, uncertainties in the thermodynamic properties of the reaction components, uncertainties of the reaction kinetics under the wide range of operating conditions, high cost, toxicity and flammability (Gil et al., 2009; Glatzmaier, 2011).

3. SELECTION OF STORAGE TECHNOLOGY AND DESCRIPTION OF COMPONENTS OF A CENTRAL RECEIVER PLANT

3.1 Most suitable thermal storage technology for central receiver

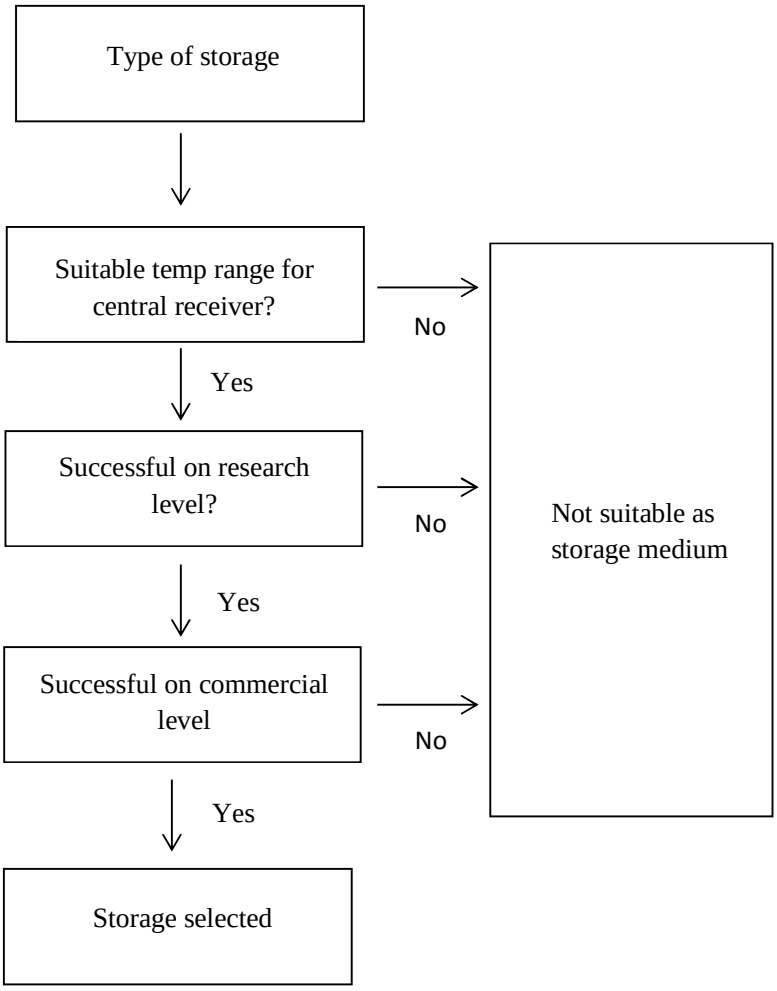

Figure 5: Decision tree for selection for storage

From the TES literature review, it is evident that latent heat and thermochemical storage are still at research level. They are therefore not viable options for use as a storage medium at a commercial level. The most advancement has been made in the field of sensible heat storage. The two-tank molten salt, single-tank thermocline and DSG systems show the greatest potential. The single-tank

thermocline and DSG systems still have technical issues that need to be addressed. The two-tank molten salt storage system has the ability to reach the highest system temperatures which increases the efficiency of the Rankine cycle. It has also made the most advancement, with a 19.9-MW_e commercial plant operating in Spain. This technology is therefore the one identified as the most suitable for use as a storage medium for commercial electricity production.

3.2 Two-tank molten salt central receiver plant

Heliostat field collectors focus sunlight to a central receiver tower to heat up the HTF. Current commercial systems use molten salt as the HTF and storage medium. The molten salt is heated and pumped to a hot storage tank where it is stored until it is required for electricity generation. When needed for electricity generation, it is pumped through the steam generator (SG) to produce steam that is utilised in a conventional Rankine cycle for the production of electricity (Tyner et al., s.a). The molten salt is then routed to the cold tank to begin the cycle again. Figure 6 is a schematic of the molten salt power tower.

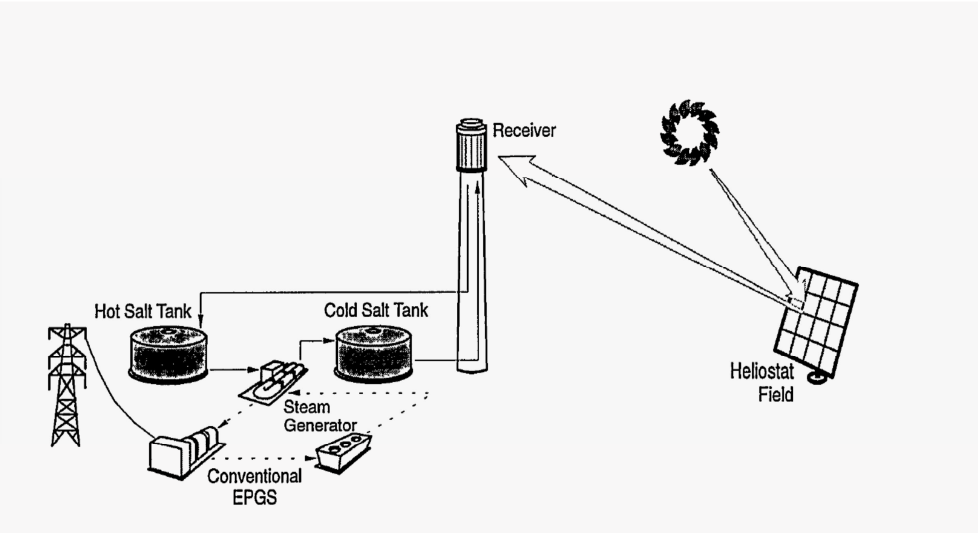

Figure 6: Molten salt power tower

Source: Tyner et al., s.a.

The design basis for the research was 100MW_e dry cooled central receiver plant with molten salt storage . The design point used was March 12 at 12:00. The resultant aperture area for a solar multiple of one at design point was calculated to be 497 325 m^2.

3.3 Description of components of concentrating solar power central receiver plant

3.3.1 Heliostat field

A heliostat is made of low-iron glass mirrors. To form a heliostat, several mirror modules are interconnected instead of using one large mirror (Figure 7). A heliostat is essentially a sun-tracking mirror, and thousands of heliostats together form the heliostat field that allows us to exploit the energy provided by the sun (Figure 8).

Figure 7: Mirror modules interconnected to form heliostat

Source: Wikipedia, 2013.

Figure 8: Gemasolar power plant in collection mode with molten salt heated at the illuminated receiver

Source: Concentrating solar energy of the future, 2011.

The heliostat field does not reflect all the energy that it intercepts from the sun toward the tower because there are losses that occur. There is some incident energy that is absorbed by the mirror surface, which can be minimised by using low-absorption glass mirrors. Losses are also experienced as a result of the heliostat field layout. Cosine losses depend on the position of the sun and the location of the individual heliostat relative to the receiver. The heliostat surface normal bisects the angle between the solar rays and a line from the heliostat to the receiver. The effective reflection area of the heliostat is reduced by the cosine of one half of this angle. Another loss factor inherent in the heliostat field is atmospheric attenuation that becomes significant when there is a large heliostat field and the outer heliostats are a great distance from the receiver. Shading (also referred to as shadowing) and blocking losses (Figure 9) further decrease the energy directed to the receiver. Shading occurs when a heliostat casts its shadow on a heliostat located behind it. Blocking is the interception of the reflected sunlight by the heliostat in front. Typical efficiency values for mirror reflectivity, field optical efficiency (accounts for cosine, blocking, shading and attenuation losses) and field availability are approximately 94%, 65% and 99% respectively **(**Sargent and Lundy LLC Consulting Group, 2003).

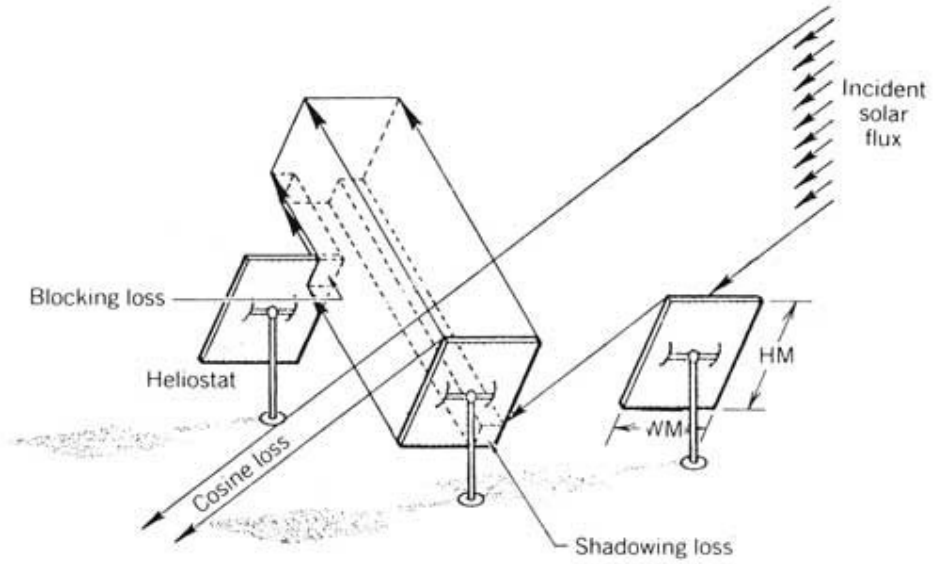

Figure 9: Cosine, shading and blocking losses experienced by heliostats

Source: Solar technology suitability review, 2012.

3.3.2 Receiver tower

The energy intercepted by the heliostats is reflected to a receiver that is placed on top of a tower. The incident energy is absorbed by the receiver and transferred to the HTF that runs through the receiver. There are two types of receiver, namely an external receiver and a cavity receiver.

The external receiver (Figure 10) is made of panels of multiple small vertical tubes welded side by side to represent a cylinder. The top and bottom of the tube are connected to headers that allow the HTF to flow through the receiver. To minimise heat loss, the receiver area is kept to a minimum, with a typical height-to-diameter ratio of 1:1 to 2:1.

In a cavity receiver, the heat-absorbing surface is placed inside an insulated cavity. This reduces the convection heat losses from the receiver. Cavity receivers have a limited acceptance angle of 60 to 120 degrees. This results in multiple cavities being placed next to each other or the heliostat field view is limited to the view of the cavity aperture.

The design of the receiver is limited by the heat flux that can be absorbed through the receiver surface into the HTF, without overheating the receiver walls or HTF.

Receivers using molten salt as the working fluid can tolerate peak flux densities in the range of 1 MW_t/m^2 (Lata et al., 2008).

Figure 10: External receiver at Gemasolar

Source: Concentrating solar energy of the future, 2011.

Not all of the energy reflected by the heliostat field onto the receiver is absorbed by the HTF. Energy losses occur, and these are attributed to convection, conduction, radiative, reflective and spillage losses (Figure 11). The convection loss is influenced by exposure to wind and the wind speed. The convection and radiation losses are functions of the receiver size and operating temperature and are highly influenced by the design of the receiver, in other words cavity or external receiver. At higher temperatures, the radiative loss becomes the most significant.

Energy from the heliostat field that is directed toward the receiver and does not fall on the absorbing surface is referred to as spillage loss. It is a function of both the heliostat field and receiver design. The spillage loss can be reduced by increasing the receiver size, but this will increase energy loss to radiation and convection. The receiver size must therefore be optimised to absorb the maximum amount of energy from the heliostat field while minimising the losses to radiation and convection.

The receiver is coated with high-absorptivity paints that are formulated for high-temperature surfaces. The absorptivity of the coating used is approximately 0.95 (Ho et al., 2013).

The conduction losses are mainly attributed to the supporting structure for the receiver. This is a small fraction of the overall heat loss from the receiver and is minimised by limiting the number and size of receiver attachment points and using low-thermal-conductivity materials such as stainless steel.

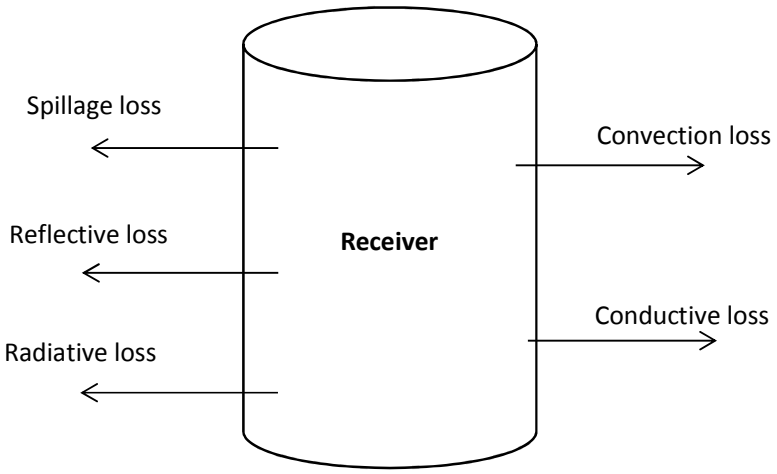

Figure 11: Receiver energy losses

3.3.3 Steam generator

The solar field storage system (molten salt) and electricity generation system (power block) can be seen as two independent systems interconnected by the SG, as shown in Figure 12. Salt from the hot storage tank is passed through the SG where it heats the incoming feedwater to superheated steam that is expanded through the turbine to produce electricity. The steam generation system consists of a preheater, evaporator, superheater and reheater (Figure 13). The feedwater is fed into the preheater where the lower temperature salt that has already passed through the superheater and evaporator is used to heat the pressurised feedwater to just below the temperature at which evaporation occurs. In the evaporator, the medium-temperature salt that has passed through the superheater is used to convert the feedwater to saturated steam. In the superheater, the high-temperature salt that comes from the hot salt tank is used to superheat the steam that is generated in the evaporator.

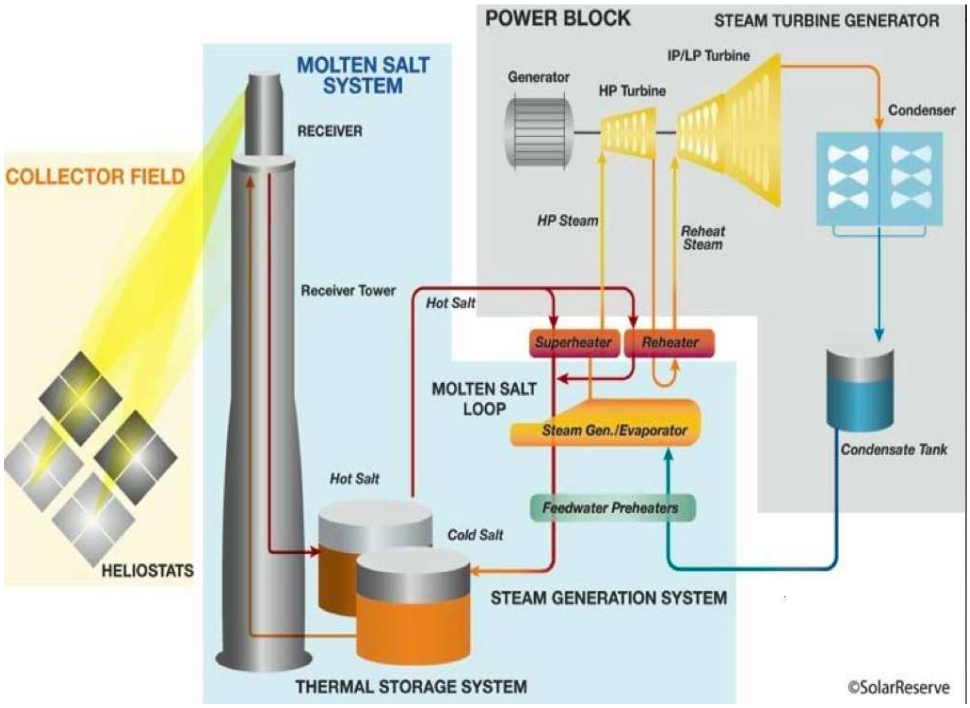

Figure 12: Solar field and power block linked by steam generator

Source: Jones, 2012.

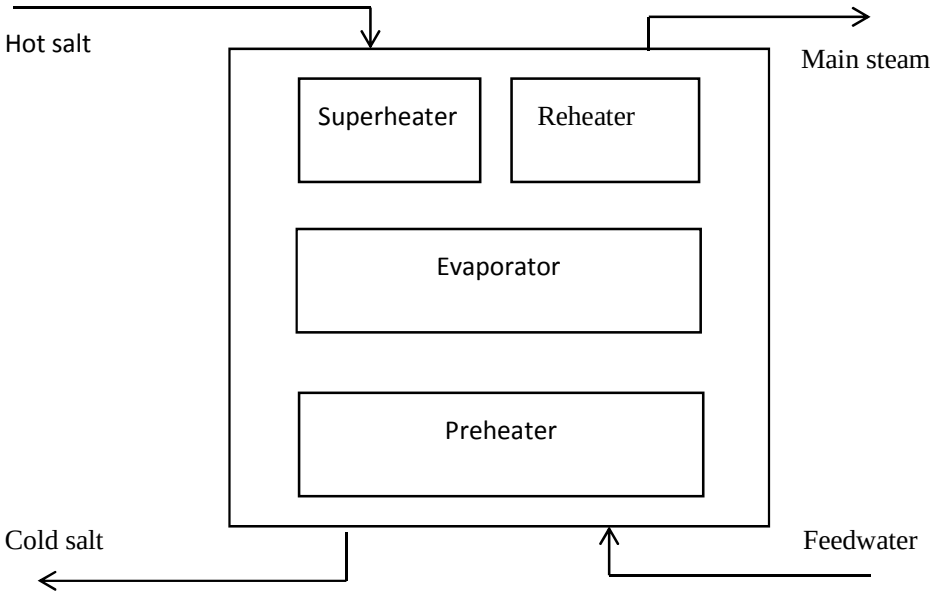

Figure 13: Schematic of steam generator

A temperature-heat recovery diagram as shown in Figure 14 can be used to illustrate the three phases of heat transfer.

The upper line shows the cooling of the salt from the input to the output of the SG. The lower line represents the process of converting water into steam. The pinch point temperature difference is the difference between the temperature of the salt exiting the evaporator and the temperature at which evaporation of the feedwater occurs. The pinch point temperature difference is usually between 5 ˚C and 15 ˚C. A lower pinch point would result in more heat being extracted from the salt but an increase in the cost of the heat exchanger. It is an important parameter when designing a SG. The use of the pinch point when designing a SG avoids a temperature cross situation. A temperature cross situation is undesirable and occurs when part of the preheater and part of the evaporator virtually heat the salt. A temperature cross situation shown in Figure 15 can present itself if the exit salt temperature is assumed without checking the pinch point difference.

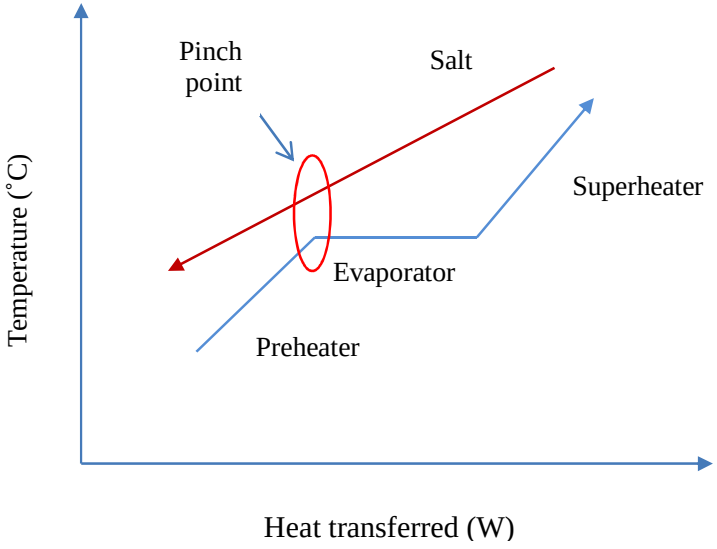

Figure 14: Temperature-heat recovery diagram depicting pinch point

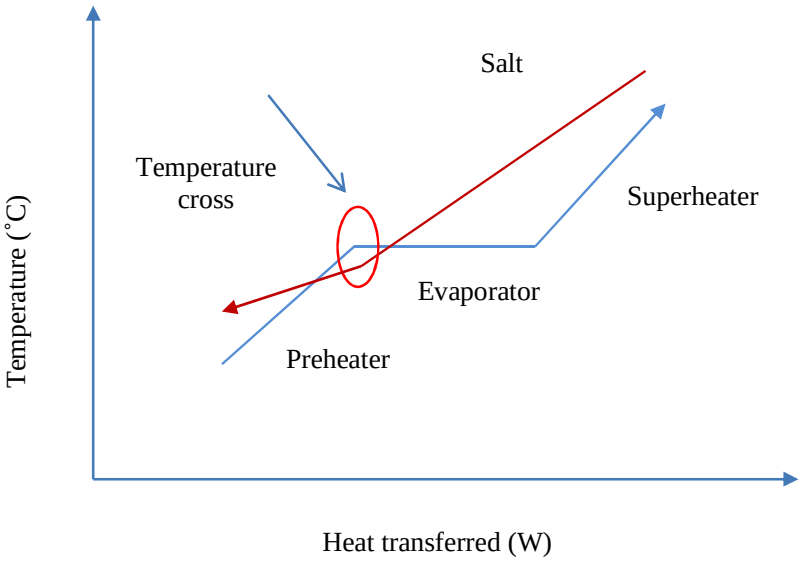

Figure 15: Temperature-heat recovery diagram showing temperature cross situation

3.3.4 Power block

The ideal Rankine cycle on the T-s diagram in Figure 16 does not involve any irreversibilities within the components and interconnecting piping and consists of the following four processes.

1-2: isentropic pressure rise in a pump

2-3: constant pressure heat addition in a SG

3-4: isentropic expansion in a turbine

4-1: constant pressure heat rejection in a condenser

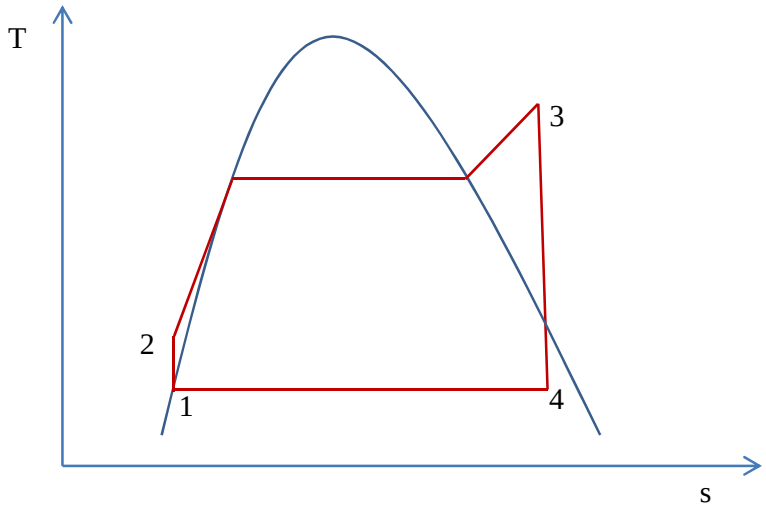

Figure 16: Schematic of simple ideal Rankine cycle

In reality there are irreversibilities in the various components, which result in the actual vapour power cycle differing from the ideal Rankine cycle. Two common sources of irreversibilities are fluid friction and heat loss to the surroundings. Fluid friction causes pressure drops across the components and in the associated piping. To accommodate the pressure loss across the SG and the piping leading to the turbine inlet, the feedwater pumps raise the pressure sufficiently above that which is required at the turbine inlet.

As the steam flows through the various components, heat is lost to the surroundings, thus to maintain the same network output, more heat is transferred to the steam in the SG. This results in a decrease in the cycle efficiency.

As a consequence of the irreversibilities, the pump requires a greater work input and a lower work output is produced by the turbine. The resulting T-s diagram is shown in Figure 17.

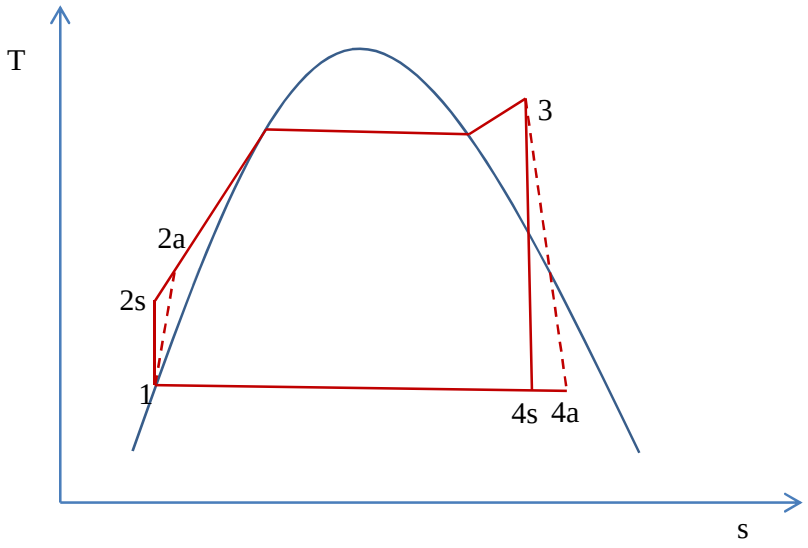

Figure 17: Effect of pump and turbine irreversibilities on Rankine cycle

3.3.4.1 Increasing the efficiency of the Rankine cycle

Increasing the average temperature at which heat is transferred to the working fluid in the SG or decreasing the average temperature at which heat is rejected from the working fluid in the condenser improves the efficiency of the Rankine cycle. This is achieved by means of the following:

a) Superheating the steam to high temperatures: Keeping the SG pressure constant and superheating the steam increase the average temperature at which heat is added to the working fluid.
b) Increasing the SG pressure: Increasing the operating pressure of the SG automatically raises the temperature at which boiling takes place, which

increases the average temperature at which heat is added and raises the thermal efficiency of the cycle.

c) Lowering the condenser pressure: Operating the condenser at a lower pressure results in the heat being rejected at a lower temperature.

There are limitations to the above. Lowering the condenser pressure increases the possibility of air leakage into the condenser. There is also an increase in the moisture content of the steam in the final stages of the turbine. Superheating the steam addresses the issue of moisture content in the final stages of the turbine.

There is a limit to the degree of superheating that is possible with the steam due to limitations experienced by the materials used. With current materials, the highest steam temperature allowed at the turbine inlet is approximately 620 ˚C. Surpassing 620 ˚C becomes a trade-off between costs of efficiency improvements and materials costs.

For a fixed turbine inlet temperature, an increase in the SG pressure increases the moisture content of the steam at the turbine exit. This is undesirable and is corrected by reheating the steam.

3.3.4.2 The reheat Rankine cycle

Increasing the SG pressure increases the thermal efficiency of the Rankine cycle with the negative effect of increasing the moisture content of the steam in the final stages of the turbine. There are two possibilities for taking advantage of the gain in thermal efficiency:

a) Superheating the steam to very high temperatures: This raises the average temperature at which heat is added, thus increasing the thermal efficiency. This has metallurgical limitations and is hence not a viable solution.
b) Using two turbine stages to expand the steam, reheating the steam in between the two stages: Reheating is a commonly used practice in modern power stages to resolve the problem of excessive moisture in the final stages of the turbine.

The reheat cycle in Figure 18 differs from the simple Rankine cycle in that the expansion through the turbine occurs in two stages. The steam is partially expanded in the high-pressure turbine, and this intermediate-pressure steam is returned to the SG where it is reheated at constant pressure to the inlet temperature of the high-pressure turbine. This steam is then sent to the second-stage turbine where it is expanded to the condenser pressure. The optimum reheat pressure is about one quarter the maximum cycle pressure (Çengel & Boles, 2011).

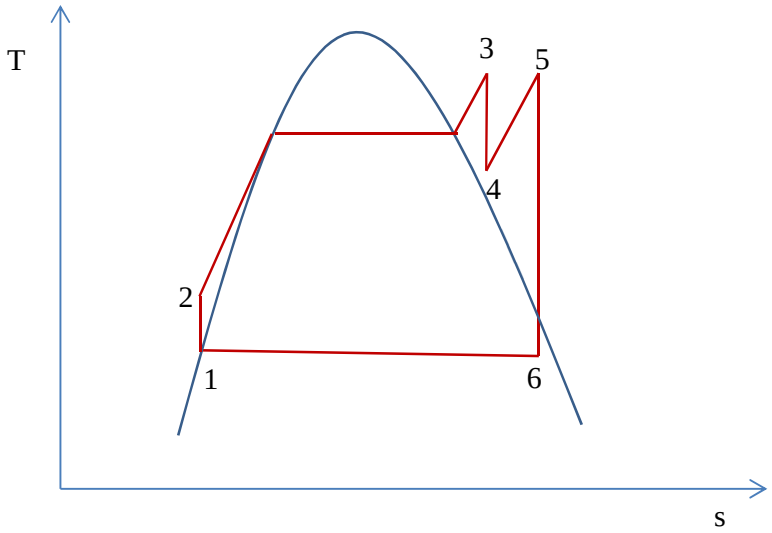

Figure 18: The reheat Rankine cycle

3.3.4.3 The regenerative Rankine cycle

The regenerative Rankine cycle (Figure 19) increases the SG input temperature, which results in an increase in the average temperature at which heat is added. This is accomplished by feedwater preheating. Small amounts of steam are extracted from the turbine at various points and used to heat the feedwater before it enters the SG. If a very large number of extraction stages and feedwater heaters are used, the cycle efficiency would approach that of the idealised regeneration cycle (Van Wylen & Sonntag, 1978). This produces less turbine work per unit mass flow as the steam is prevented from expanding but increases the efficiency of the overall cycle. The number of extraction stages becomes a trade-off between the savings effected by the increase in efficiency and the cost of the additional equipment required for feedwater heaters.

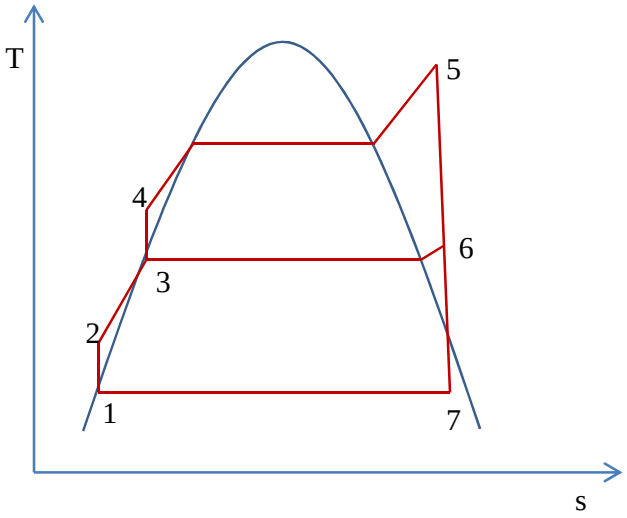

Figure 19: T-s diagram of an ideal regenerative Rankine cycle with one open feedwater heater

In addition to increasing the cycle efficiency, regeneration also allows the removal of air that leaks into the condenser (de-aeration), thereby preventing corrosion in the SG.

4. COST ASSOCIATED WITH CENTRAL RECEIVER

4.1 Concentrating solar power receiver plant cost

Central receiver power plants are capital intensive with virtually zero fuel cost. The infancy of the technology results in limited references to determine the investment cost of central receiver power plants. The best available reference with respect to costs associated with receiver plants is data published by NREL, Sargent and Lundy LLC Consulting Group and the International Renewable Energy Agency.

Table 1 shows the direct cost of CSP plants broken down into different categories (Sargent & Lundy LLC Consulting Group, 2003).

Table 1: Cost estimates by Sunlab and Sargent and Lundy

	Sunlab	**Sargent and Lundy**
Structures and improvements, $/m^2 field	12.3	11.6
Heliostat field, $/m^2 field [*,•]	200	200
Receiver, $k/m^2 receiver	50	57.1
Tower and piping, $/m^2 field	12.1	11.6
Thermal storage, $/kW$_t$	49	49
Steam generator, $/kW$_t$	14	14
Electric power, $/kW$_e$	733	557
Balance of plant $/kW$_e$	532	733
Indirect costs, $/kW$_e$	440	1 134
Contingency, $/kW$_e$	453	890
Risk pool, $/kW$_e$	580	642

Source: Sargent and Lundy LLC Consulting Group, 2003.

[*] Personal communication with Xavier García-Casals (2013) revealed that a heliostat cost of $\$200/m^2$ was a more realistic value.
[•] Turchi et al., 2010.

4.2 Levelised electricity cost (LEC)

The levelised cost of electricity is calculated using Equation 4.1 (International Renewable Energy Agency, 2012b) and is the price at which electricity must be generated from a specific source to break even over the lifetime of the project.

$$LEC = \frac{\sum_{t=1}^{n} \frac{I_t + M_t + F_t}{(1+r)^t}}{\sum_{t=1}^{n} \frac{E_t}{(1+r)^t}} \qquad (4.1)$$

The quality of the solar resource and the capital cost of the plant are highly influential to the outcome of the LEC calculation. Assuming a base DNI of 2 100 kWh/m^2/yr (typical for Spain), the expected LEC of a CSP plant is expected to decline by 4.5% for every 100 kWh/m^2/yr that the DNI exceeds 2 100 (International Renewable Energy Agency, 2012b). The initial investment cost accounts for approximately four fifths of the total cost. Including TES increases the specific investment cost due to inclusion of the storage system and the associated increase in the size of the solar field. The resultant increase in electricity generation will, however, result in a lower LEC. Capital cost estimates for a plant with storage range from \$6 300/kW to \$10 500/kW. The resultant levelised cost of electricity falls between \$0.14/kWh and \$0.29/kWh, and in areas with an excellent solar resource, this could be as low as \$0.14/kWh to \$0.18/kWh (International Renewable Energy Agency, 2012b). The cost of electricity from CSP is currently higher than conventional fossil fuel technologies.

The LEC of CSP plants are influenced by the following key parameters:

- The initial investment cost, including site development, components and system, assembly, grid connection and financing costs.
- The capacity factor and efficiency of the plant.
- The local DNI at the plant site.
- The operation and maintenance (O&M) costs (excluding houseload).
- The cost of capital, economic lifetime.

To determine the LEC the Sargent and Lundy values were multiplied by their respective cost categories from the plant model to determine the investment cost. The Sunlab values were used as comparison. To convert to Rands a R/\$ exchange rate was estimated to be R9/\$ (2012). The plant life was assumed to be 25 years and the discount rate was assumed to be 5.6%. The operation and maintenance

costs were derived from data published by NREL. The electricity generated annually was determined from the plant model.

4.3 Cost reductions for concentrating solar power plants

The use of CSP for the generation of commercial power is still in its early stages, and this provides many opportunities for cost reduction. The use of cheaper components, improvements in design and mass production can decrease the costs associated with the solar field. Utilising HTF capable of achieving higher temperatures and cost reductions in storage is also possible (International Renewable Energy Agency, 2012b). As the technology matures, it is anticipated that capital cost reductions of 10% to 15% and reductions in O&M costs could see the LEC of solar towers decline to between $0.15/kWh and $0.24/kWh. The reductions in cost will be as a result of economies of scale in the plant size and manufacturing industry. It is envisaged that by 2020, capital cost reductions of 28% to 40% could be achieved (International Renewable Energy Agency, 2012b).

5. MODELLING

5.1 Modelling platform

Using hourly typical meteorological year (TMY) data for Upington, a macro-level hourly steady-state efficiency-based power plant model was created using Microsoft Excel. The model was developed for a 100-MW_e, dry-cooled central receiver plant with two-tank molten salt storage. The model provided an estimate of annual power output and allowed one to determine the effect of changing various parameters on the annual energy output that influenced the LEC. The design point was 20 March, 12:00.

5.2 Plant components

The plant model consisted of the following components:

- Heliostat field
- Receiver
- Storage tanks
- SG
- Power block

5.3 Model description

5.3.1 Heliostat field

To determine the heliostat field efficiency, Equation 5.1, which is dependent on the zenith angle (Figure 20) and accounts for cosine, shading and blocking effects, was used (Gauche et al., 2011).

$$\eta_{optical} = 0.4254\theta_z^6 - 1.148\theta_z^5 + 0.3507\theta_z^4 + 0.755\theta_z^3 - 0.5918\theta_z^2 + 0.0816\theta_z + 0.832 \quad (5.1)$$

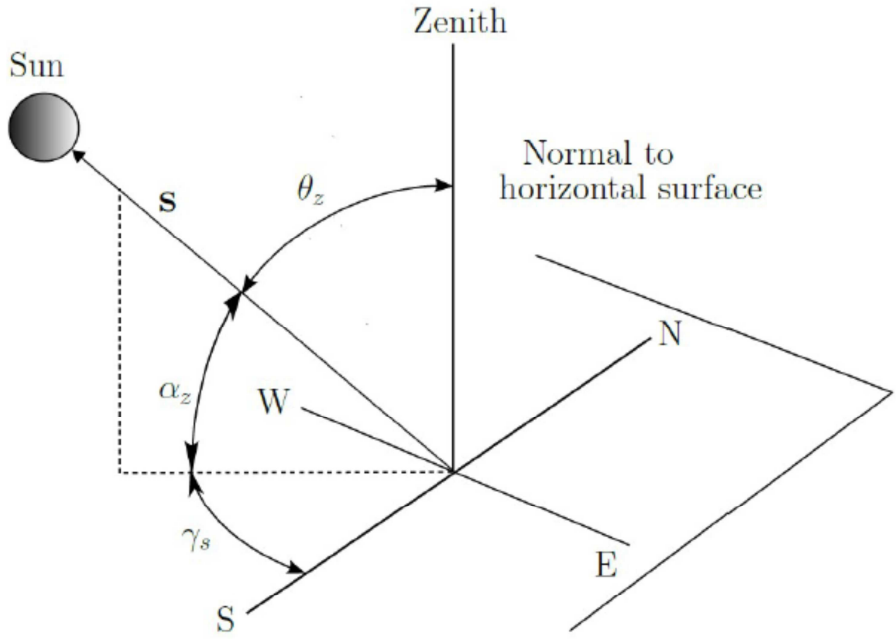

Figure 20: Schematic showing sun angles

To determine the zenith angle, the solar time needs to be calculated and this allows one to calculate the hour angle, which is required for the zenith angle calculation. The solar time is calculated as follows:

$$\text{Solar time} = \text{Standard time} + \frac{[4(L_{st} - L_{loc}) + E]}{60} - 0.5 \qquad (5.2)$$

The standard time and solar time are in hours while E, which represents the equation of time, is in minutes and is represented by

$$E = 229.2(0.000075 + 0.001868\cos B - 0.032077\sin B - 0.014615\cos 2B - 0.04089\sin 2B) \qquad (5.3)$$

B represents the day of the year in angular value and is determined using

$$B = \frac{(n_1 - 1)360}{365} \qquad (5.4)$$

The solar time is used to calculate the hour angle, which indicates the position of the sun with respect to the meridian, as follows:

$$\omega = [Solar\ time - 12](15) \qquad (5.5)$$

The angle of declination is additionally required and is calculated as follows:

$$\delta = 0.006918 - 0.399912\cos B + 0.070257\sin B - 0.006758\cos 2B + 0.000907\sin 2B - 0.002679\cos 3B + 0.00148\sin 3B \quad (5.6)$$

The parameters calculated above are used to calculate the zenith angle as follows:

$$\theta_z = cos^{-1}[\cos\phi\cos\delta\cos\omega + \sin\phi\sin\delta] \quad (5.7)$$

5.3.2 Receiver

To determine the optical energy that is incident on the receiver, heliostat fouling, reflectivity, availability and spillage need to be accounted for. From Section 3.3.1, one can see that field efficiency is approximately 65%. It is assumed that 15% of the reflected energy is lost to spillage and attenuation, which results in a design point efficiency of 65%. This is captured as follows:

$$Receiver\ opt\ eff = (Heliostat\ avail)(Heliostat\ fouling)(Heliostat\ refl)(Heliostat\ opt\ eff)(1 - spill) \quad (5.8)$$

Data from NREL indicate that the receiver area for a 100-MW_e CSP receiver plant is expected to be 1 110 m^2 (Sargent & Lundy LLC Consulting Group, 2003). The Excel model was developed for a receiver surface area of 1 000 m^2. The total energy incident on the receiver is determined as follows:

$$Q_{receiver\ in} = (Receiver\ absorbtivity)\ (DNI)(Receiver\ opt\ eff\ )(Field\ aperture)(SM) \quad (5.9)$$

The heat flux possible on the receiver limits the amount of energy that can be incident on the receiver. This is assumed to be 700 kW_t/m^2 (Sargent & Lundy LLC Consulting Group, 2003).

$$Max\ energy\ absorbed\ by\ receiver = (Max\ allowable\ heat\ flux)(Receiver\ surface\ area) \quad (5.10)$$

The receiver experiences thermal energy losses due to convection and radiation. To determine the convective loss, a convective heat transfer coefficient is determined using Equation 5.11 (Duffie & Beckman, 2006). An energy balance is performed using the receiver average temperature, with the receiver outlet

temperature being set to its rating, assuming that flow rate will be calculated accordingly (Gauche et al., 2011). The ambient temperature was obtained from the site TMY data.

Convection loss

$$h = 2.8 + 3V \tag{5.11}$$

$$Q_{conv} = hA(T_r - T_a) \tag{5.12}$$

Radiation loss

$$Q_{rad} = \varepsilon A\sigma(T_r^4 - T_a^4) \tag{5.13}$$

A receiver energy balance (Figure 21) enables one to determine the net energy (Q_{net}) that is transferred to the salt and sent to storage.

Figure 21: Receiver energy balance

$$Q_{net} = Q_{receiver\ in} - Q_{conv} - Q_{rad} \tag{5.14}$$

5.3.3 Storage

The storage system was modelled as being 98.5% efficient (Sioshansi et al., 2010). This implies that for an hour, 1.5% of the energy in storage is lost to the surrounding environment. To determine the amount of thermal energy required for an hour of storage, the design point data are examined.

$$\frac{Energy\ Stored}{3\,600\ s} = \frac{Gross\ Power\ Output}{Reference\ Power\ Block\ Efficiency} \tag{5.15}$$

5.3.4 Steam generator

Figure 22 shows a schematic of the SG layout. The salt flow through the superheater and reheater is in parallel and the salt flow rate through the reheater and superheater is configured to allow the exit temperature from both components to be equal. The pressure drop across the preheater, evaporator and superheater is assumed to be equal. By using the evaporator and superheater pressure, the saturation temperature at the entrance to these components is determined. The temperature at the evaporator entrance is then set at a delta T below the saturation temperature (e.g. at 146.67 bar, the sat temp is 340.36 ˚C; the temperature at the evaporator entrance is set at 340.36 – 5 = 335.36 ˚C). At the evaporator exit, the saturation temperature is looked at and a delta T is added. (e.g. at 153.33 bar, the sat temp is 343.92 ˚C.) The temperature at evaporator exit is set at 343.92 + 1 = 344.92 ˚C. Knowing the input and output feedwater conditions across the preheater evaporator, superheater and reheater, the energy requirement across each component can be calculated by

$$Q = \dot{m}(h_{out} - h_{in}) \qquad (5.16)$$

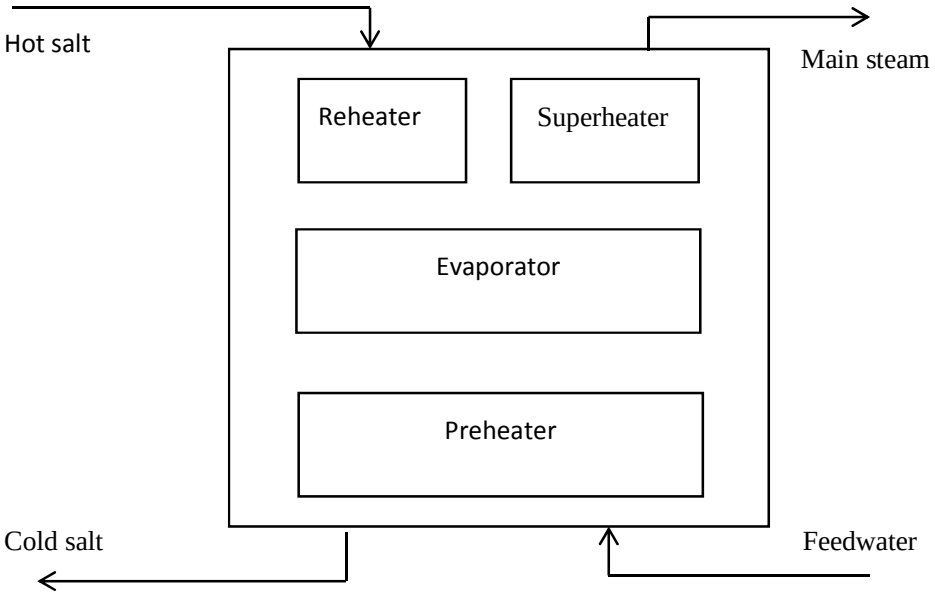

Figure 22: Steam generator (SG) layout (Figure 13 repeated for convenience)

The input and output salt temperature across the SG is known, and the input feedwater and main steam conditions are obtained from the turbine/feedheating

model. An energy balance is performed on the SG to determine the required salt flow rate. The specific heat capacity of the salt is determined at the average salt temperature by using the temperature-dependent heat capacity equation (Appendix B).

$$\dot{m}_{salt} = \frac{\dot{m}_{feedwater}(h_{main\ steam} - h_{feedwater})}{C_p(T_{hot\ salt} - T_{cold\ salt})} \quad (5.17)$$

Isolating each component within the SG and performing an energy balance enable calculation of the exit salt temperature from each component. The energy requirement across each component is determined by Equation 5.16. The flow through the superheater and reheater is manipulated to allow the same exit temperature.

5.3.5 Power block

A steady-state single reheat regenerative Rankine cycle power block model as shown in Figure 23 was developed with reference to the *Fundamentals of Engineering Thermodynamics* (Moran & Shapiro, 2006). Microsoft Excel was the software platform used. The add-in X Steam was used for the thermodynamic properties of water and steam. It is based on the International Association for Properties of Water and Steam Industrial Formulation 1997 (IAPWS IF-97). All forward and backward functions are programmed. Using pressure and temperature, pressure and entropy or entropy and enthalpy, all properties can be calculated. The power block consists of the following components:

- SG
- Turbine
- Electrical generator
- Condenser
- Feedwater system including feedpumps

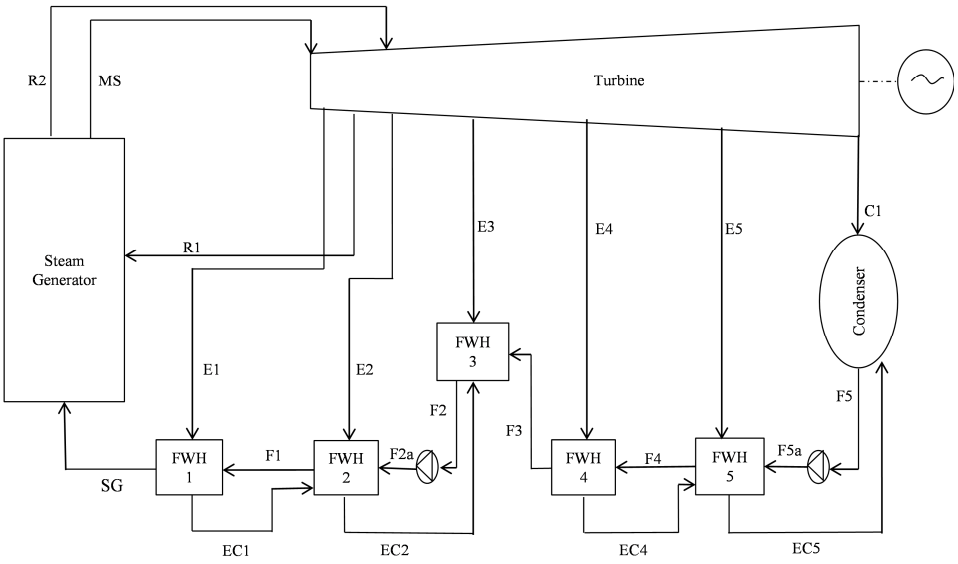

Figure 23: Power block feedwater heating layout with five feedwater heaters

The output of one component is taken as the input of the downstream component. The optimum reheat pressure is assumed to be one quarter of the maximum cycle pressure (Çengel & Boles, 2011). The isentropic efficiency of the turbine is assumed to be 85%.

The heating arrangement for medium-capacity turbines and high-pressure, high-capacity turbines is between 3–7 heaters (Rajput, 2007). The operating pressure range of current CSP turbines is between 100 and 140 bar (Siemens, 2010). The power block was modelled with 4–6 heaters to determine the effect on efficiency. The feedwater pressure and temperature were varied between 100 and 140 bar and 200 and 40 ˚C respectively. The model is executed as an hourly steady state model with a dry-cooled condenser, and as such the steam flow rates will change for every hour. The condenser pressure is determined by

$$P_{condenser} = P_{sat}(T_{db} + ITD) \qquad (5.18)$$

where ITD is the initial temperature difference of 20 ˚C (Hoffmann, 2012).

It is accepted that an ITD of 20 ˚C is to a certain degree optimistic. In reality a smaller ITD results in a larger and more expensive plant. The costing data used does not account for the differences in the ITD, and hence an ITD of 20 ˚C was used.

The feedwater input conditions and the main steam conditions are controlled. It is assumed that the temperature rise (Equation 5.19) across each feedwater heater is equal (Nag, 2007). The outlet temperature of each feedwater heater can hence be calculated.

$$Temperature\ rise = \frac{feedwater\ input\ temp - condenser\ exit\ temp}{number\ of\ feedwater\ heaters} \quad (5.19)$$

Steam generator (SG to MS)

The turbine main steam conditions will be used as the starting point. The feedwater input conditions to the SG are known. The thermal input required from the SG (excluding reheater) can be calculated by taking the enthalpy difference between the between the main steam and feedwater:

$$q_{SG,in} = (h_{MS} - h_{SG}) \quad (5.20)$$

Reheater (R1 to R2)

The reheater pressure is taken as one quarter of HP turbine inlet pressure and the reheat temperature is equal to the HP turbine inlet temperature. Steam is extracted at the HP turbine outlet for regenerative heating. The heat input per unit mass required from the reheater is given by

$$\frac{q_{RH,in}}{\dot{m}_{MS}} = h_{R2} - h_{R1} \quad (5.21)$$

HP turbine (MS to R1)

The isentropic efficiency is considered to be 0.85 for all stages of the turbine. The work rate output per unit mass of the turbine is determined by

$$\frac{w_{t1}}{\dot{m}_{MS}} = h_{MS} - h_{R1}$$

where $h_{R1} = h_{MS} - 0.85(h_{MS} - h_{R1,is})$ (5.22)

IP/LP turbine (R2 to E1, E2, E3, E4, E5, C1)

To determine the extraction points (E1 to E5), the outlet temperature of each feedwater heater is examined. A delta T (5 ˚C) is added to the outlet temperature. The saturated temperature of the extracted steam is related to this new temperature. For Feedwater Heater 1, the exit temperature is 220 ˚C, hence the extracted steams saturated temperature is 225 ˚C (220 ˚C + 5 ˚C). The extraction pressure is determined at this new temperature.

The work output per unit mass for Turbine 2 is determined by

$$\frac{w_{t2}}{\dot{m}_{MS}} = \dot{m}_{E1}(h_{R2} - h_{E1}) + \dot{m}_{E2}(h_{R2} - h_{E2}) + \dot{m}_{E3}(h_{R2} - h_{E3}) + \dot{m}_{E4}(h_{R2} - h_{E4}) + \dot{m}_{E5}(h_{R2} - h_{E5}) + \dot{m}_{C1}(h_{R2} - h_{C1}) \quad (5.23)$$

Condenser (C1 to F5)

The condenser is assumed to be dry cooled, and the condenser pressure is linked to the ambient temperature with an initial temperature difference of 20 ˚C. At design point the condenser pressure is 0.119 bar. The LP turbine outlet (C1) is condensed to saturated liquid (F5). The feedwater heating system is modelled as a down-cascading type whereby the extracted condensate steam is fed to the downstream feedheater to allow heat exchange to occur. This results in some of the condensed extracted steam being fed to the condenser for the heat to be rejected. The condenser heat rejected is calculated by

$$\frac{q_{out,condenser}}{\dot{m}_{MS}} = \dot{m}_{C1}(h_{C1} - h_{F5}) + \dot{m}_{EC5}(h_{EC5} - h_{F5}) \quad (5.24)$$

h_{F5} is the saturated liquid enthalpy based on the pressure (0.119 bar).

Mass flow rates for extraction points

To determine the mass flow rates, a single control volume is taken to enclose both turbine stages. Isolating Feedwater Heater 1 and performing a mass and energy balance results in

$$\frac{\dot{m}_{E1}}{\dot{m}_{MS}} = \frac{h_{SG} - h_{F2}}{h_{E1} - h_{EC1}} \quad (5.25)$$

The mass flow rates for E2 to E5 are calculated in a similar manner.

Pump work

The pumps are assumed to be isentropic. The condensate extraction pump raises the pressure to the pressure of the open feedwater heater (FWH3). The work required by Pump 1 (CEX) per unit mass is

$$\frac{w_{p1}}{\dot{m}_{MS}} = \dot{m}_{F5}(h_{F5a} - h_{F5}) \quad (5.26)$$

The SG feed pump raises the pressure to the SG input pressure. The work required by Pump 2 is

$$\frac{w_{p2}}{\dot{m}_{MS}} = \dot{m}_{F5}(h_{F2a} - h_{F3}) \quad (5.27)$$

Gross thermal efficiency

The gross thermal efficiency is determined by calculating the ratio of the net work produced to the energy input:

$$\eta_{thermal} = \frac{w_{t1}+w_{t2}}{SG\ heat\ input} \quad (5.28)$$

where SG heat input is obtained by adding Equation 5.20 and Equation 5.21.

Calculation of total mass flow rate

For a gross diagram output of 100 MW_e the total mass flow rate of steam is calculated by

$$\dot{m}_{MS} = \frac{(100)(1000)}{w_{t1}+w_{t2}} \quad (5.29)$$

5.3.6 Number of heliostats for solar multiple of one at design point

To calculate the number of heliostats required for a solar multiple of one, the efficiency of the different components is used. The total aperture area required for SM = 1 is determined by

$$Energy\ from\ Solar\ Field = \frac{Storage_{1\ hour}}{(Ref\ Receiver\ Opt\ Eff)(Reference\ receiver\ thermal\ eff)(Receiver\ absorbtivity)} \quad (5.29a)$$

$$Field\ Aperture = \frac{Energy\ from\ Solar\ Field}{Reference\ DNI} \quad (5.30)$$

The number of heliostats is determined by

$$Number\ of\ Heliostats_{SM1} = \frac{Heliostat\ Aperture\ Area_{SM1}}{Heliostat\ Size} \quad (5.31)$$

For an increase in solar multiple, the values obtained at design point are multiplied by the new solar multiple:

$$Number\ of\ Heliostats_{SM2} = (2)\ (Number\ of\ Heliostats_{SM1}) \quad (5.32)$$

5.3.7 Calculation of levelised electricity cost

For calculation of the LEC, the power plant investment cost and the energy generated per annum are required. For the investment cost, the outputs generated

from the Excel model are multiplied by their respective cost category, as shown in Table 1 in Section 4.1. The annual energy generated is obtained from the Excel model. O&M costs are calculated from data shown in Table 1, and 10% p.a. inflation is included from Year 2 onwards. It is assumed that a 100% loan is obtained at an interest rate of 10% with loan duration of 25 years. The discount rate is assumed to be equal to 5.6%. The rand-dollar exchange rate used is R/$ = 9 (2012). The annual payment is determined using the PMT function in Excel. The annual cost is obtained by adding the O&M costs and the annual payment. The enumerator and denominator are separately calculated and the LEC is determined by dividing the enumerator by the denominator.

6. MODEL VALIDATION

The plant model developed was a combination of two separate systems: the solar-field-to-storage system and the storage-to-power-block system. These two systems were integrated by the SG. The model was validated on a piecewise basis; in other words, the solar field was validated separately from the power block model.

6.1 Solar field validation

Annual TMY data for Gemasolar were obtained using Meteonorm. The annual DNI from the data obtained using Meteonorm software equates to 1 900 kWh/m^2/yr whereas NREL suggests approximately 2 150 kWh/m^2/yr for the same site (Gemasolar Thermosolar Plant, 2011). To cater for the variance, the DNI data obtained were multiplied by a correction factor of 1.131 $\left(\frac{2150}{1900}\right)$. This brought the annual DNI to 2 150 kWh/m^2/yr. The TMY data were input into the solar field model with a solar multiple of 2.5, receiver surface area of 400 m^2 and 15 hours of storage. Table 2 shows a comparison of results obtained and actual plant data. The cost data of Sargent and Lundy LLC Consulting Group (2003) were used as this resulted in a smaller variance between the calculated value and the actual Gemasolar plant cost.

Table 2: Comparison of solar field output to Gemasolar data

	Model output	**Gemasolar**	**% variance**
Heliostat aperture area (m^2)	329 770	304 750	8.21
Number of heliostats	2 749	2 650	3.74
Capacity factor (%)	70.19	74	-3.81
Input cost ($ million)	$211	$247*	-14.57

* **Source: Gemasolar Thermosolar Plant (s.a).**

6.2 Power block validation

STEAM PRO, a heat balance program specifically intended for the design of steam power cycles, was used to develop models for different power block conditions. The scope and level of detail in STEAM PRO have been continuously growing since 1990, to the point that the 2008 version has over 1 800 user-adjustable inputs (Thermoflow, 2013). STEAM PRO is a commercial code and as such there is no access available to the source code. The conditions input in STEAM PRO were simulated on the Microsoft Excel-developed model. The comparison of these is shown in Figure 24 and Figure 25.

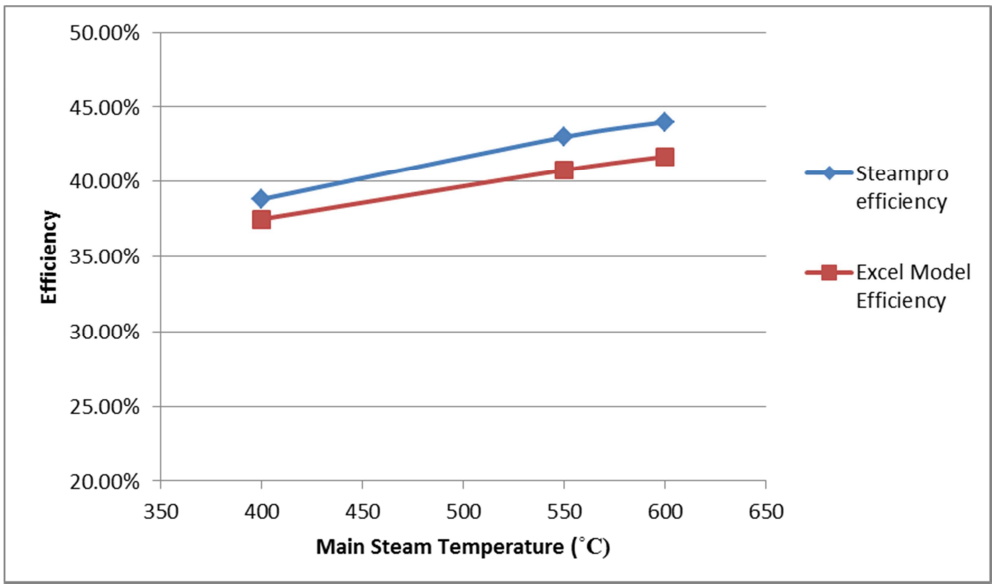

Figure 24: Comparison of efficiency from STEAM PRO model and Excel model for varying main steam temperature

Figure 24 shows that for varying main steam temperature, the outputs of the Excel model closely resemble the outputs of STEAM PRO for the same temperature and pressure conditions. The trend shown by the Excel model follows that of STEAM PRO.

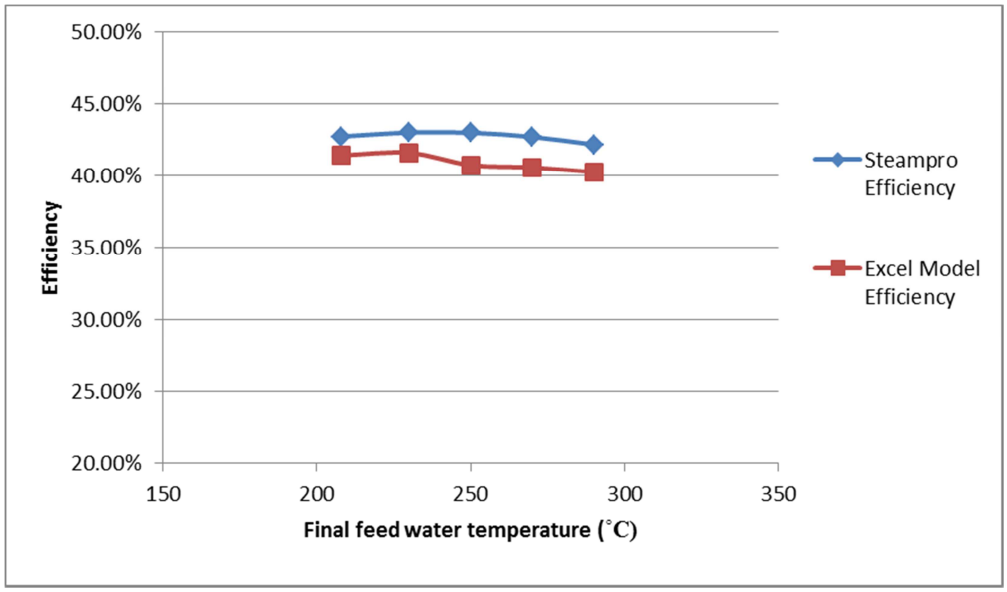

Figure 25: Comparison of efficiency from STEAM PRO model and Excel model for varying final feedwater temperature

Figure 25 shows that the STEAM PRO outputs and Excel model outputs for varying the final feedwater conditions are in close correlation. There is, however, a step that occurs between 230 ˚C and 250 ˚C. Closer inspection shows that this step is due to the fact that STEAM PRO extracts steam for the feedwater heater after the steam has expanded through the high-pressure turbine and the Excel model extracts a portion of the steam before it expands fully through the high-pressure turbine, which results in a drop in efficiency.

7. PARAMETRIC ANALYSIS TO DETERMINE EFFECT ON LEVELISED ELECTRICITY COST

The power block and solar field system are two independent systems linked together by the SG. A change in the efficiency of the power block influences the thermal capacity of the storage system and the area of the solar field. The parametric analysis investigated the effect of varying parameters that affected the power block efficiency and the effect that varying the storage capacity and increasing the solar multiple had on LEC.

7.1 Parameters to be varied

7.1.1 Power block

It follows from Section 5.3.5 that for the power block, the number of feedwater heaters was varied between three and six heaters with equal temperature rise across each feedwater heater. The feedwater temperature was varied between 200˚C – 240 ˚C in intervals of 10 ˚C. The main steam pressure was varied between 100 bar and 140 bar in 10-bar intervals.

7.1.2 Steam generator exit salt temperature

The molten salt begins to crystallise at 240 ˚C and solidifies at 220 ˚C (Kearney et al., 2002). The minimum exit salt temperature was chosen to ensure that there was no onset of crystallisation. The exit salt temperature was varied between 260 ˚C and 300 ˚C.

7.1.3 Storage time

The storage capacity was varied between six and 18 hours in two-hour intervals.

7.1.4 Solar multiple

The solar multiple was varied between 1.4 and 3.0 in increasing intervals of 0.2.

7.2 Results of parametric analysis

7.2.1 The most efficient power block configuration for different exit salt temperatures

For each exit salt temperature, the power block setup with the highest efficiency was identified. Table 3 shows the results obtained for the different exit salt temperature and changes in power block parameters.

Table 3: Power block efficiency at different exit salt temperature and power block parameters

SG exit salt temperature (°C)	Main steam pressure (bar)	SG feedwater temperature (°C)	Power block efficiency (4 FWH*)	Power block efficiency (5 FWH)	Power block efficiency (6 FWH)
260	No configuration that allows an SG pinch point greater than 5 ˚C				
270	100	210	0.4042	0.4055	0.4058
	110	210	0.4080	0.4093	0.4096
	120	200	0.4106	0.4117	0.4120
280	100	210	0.4042	0.4055	0.4058
	110	220	0.4085	0.4100	0.4103
	120	220	0.4120	0.4135	0.4138
	130	220	0.4152	0.4166	0.4169
	140	210	0.4173	0.4186	0.4189

290	100	210	0.4042	0.4055	0.4058
	110	220	0.4085	0.4100	0.4103
	120	220	0.4120	0.4135	0.4138
	130	230	0.4157	0.4173	0.4176
	140	230	0.4187	0.4203	0.4206
300	110	220	0.4085	0.4100	0.4103
	120	220	0.4120	0.4135	0.4138
	130	230	0.4157	0.4173	0.4176
	140	230	0.4187	0.4203	0.4206

*Feedwater heater.

For each exit salt temperature, the power block configuration with the highest efficiency was used to determine the effect of varying the solar multiple and storage capacity on the LEC. This is shown in Table 4.

Table 4: Power block configuration with highest efficiency at each exit salt temperature

Setup	**SG exit salt temperature (˚C)**	**Main steam pressure (bar)**	**SG feedwater temperature (˚C)**	**Power block efficiency (6 FWH)**
1.	270	120	200	0.4120
2.	280	140	210	0.4189
3.	290	140	230	0.4206
4.	300	140	230	0.4206

7.2.2 Comparison of storage capacity for different power block configurations

By using the power block configuration with the highest efficiency for each exit salt temperature, as shown in Table 4, the effect of varying the thermal storage capacity and the solar multiple was determined. Figures 26–33 show the effect of varying the solar multiple against the capacity factor and LEC for different thermal storage capacities.

Configuration 1: SG exit salt temperature 270 ˚C

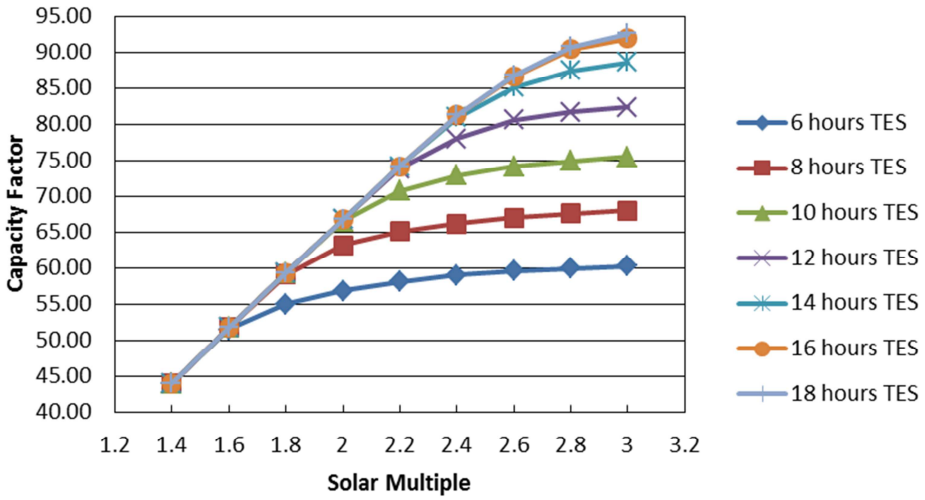

Figure 26: Capacity factor versus solar multiple for exit salt temperature of 270 ˚C

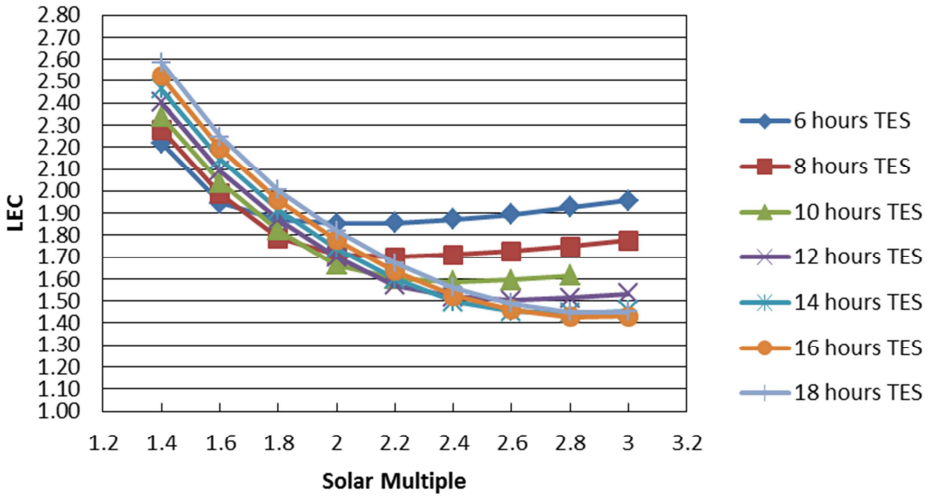

Figure 27: Levelised electricity cost versus solar multiple for exit salt temperature of 270 ˚C

Configuration 2: SG exit salt temperature 280 ˚C

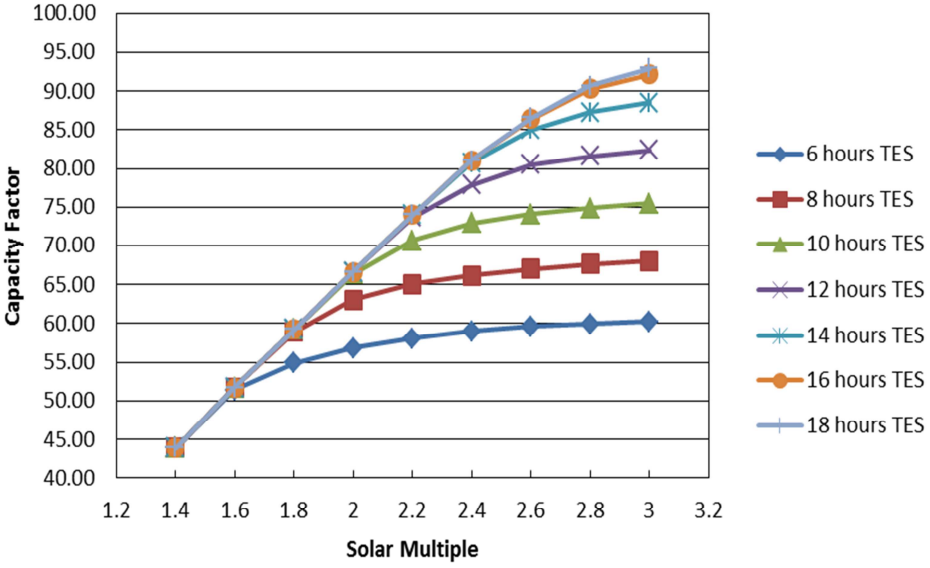

Figure 28: Capacity factor versus solar multiple for exit salt temperature of 280 ˚C

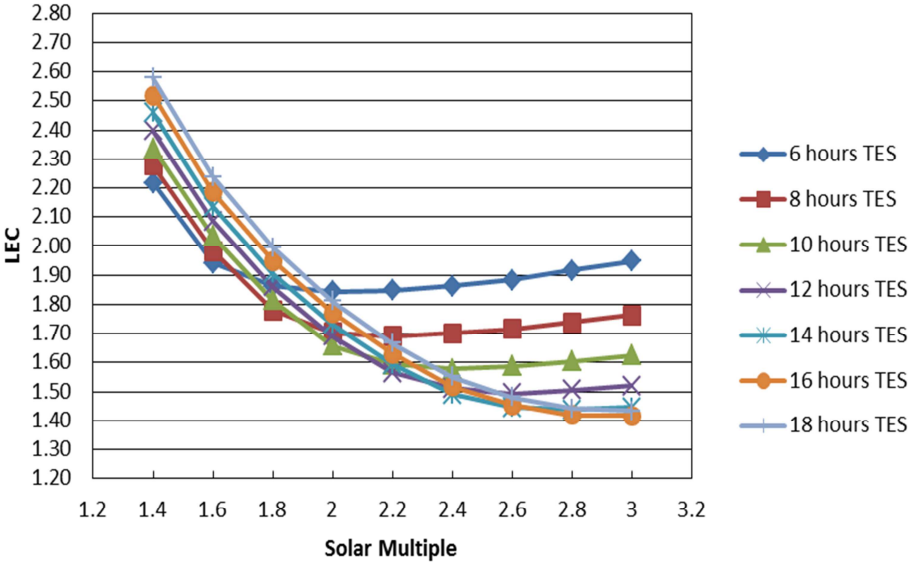

Figure 29: Levelised electricity cost versus solar multiple for exit salt temperature of 280 ˚C

Configuration 3: SG exit salt temperature 290 ˚C

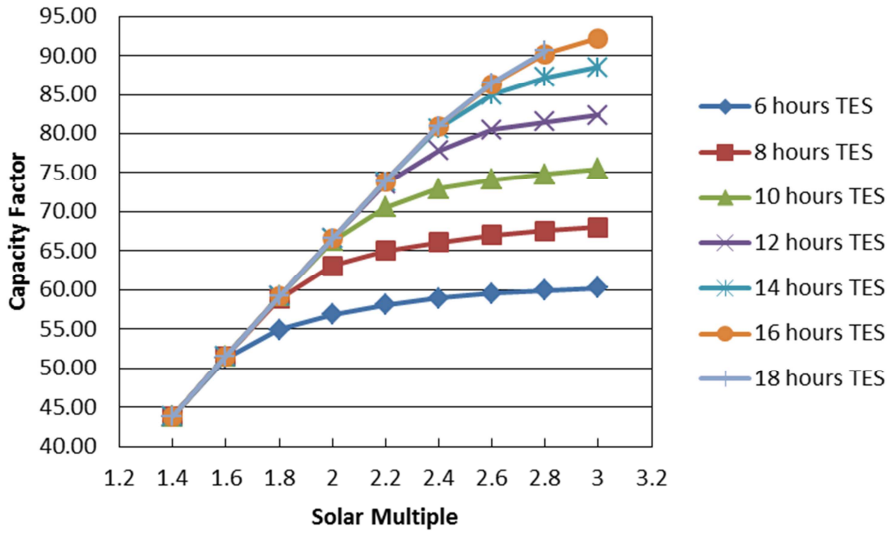

Figure 30: Capacity factor versus solar multiple for exit salt temperature of 290 ˚C

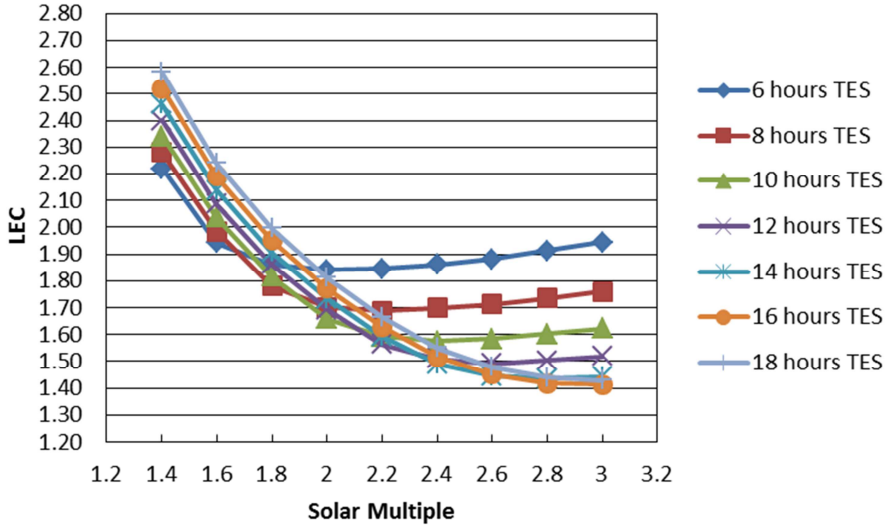

Figure 31: Levelised electricity cost versus solar multiple for exit salt temperature of 290 ˚C

Configuration 4: SG exit salt temperature 300 ˚C

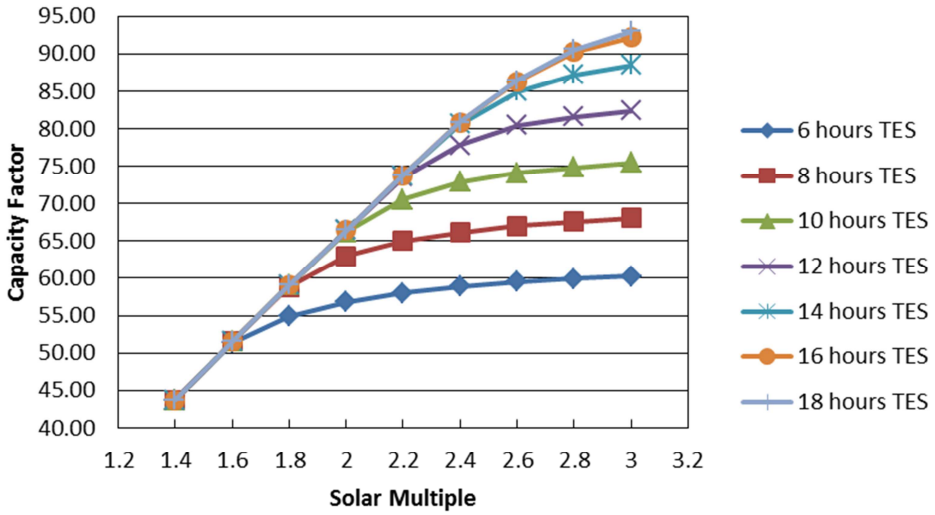

Figure 32: Capacity factor versus solar multiple for exit salt temperature of 300 ˚C

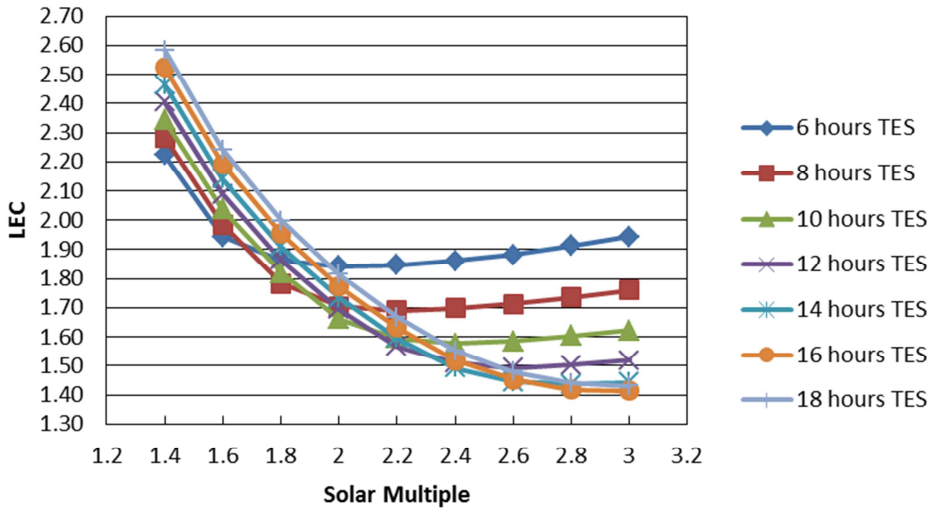

Figure 33: Levelised electricity cost versus solar multiple for exit salt temperature of 300 ˚C

7.3 Discussion of results

From Table 4 it can be seen that higher exit salt temperatures out of the SG allow the power block to be operated at a higher pressure and temperature. This results in a power block with a higher efficiency. An increase in power block efficiency results in a lower TES capacity being required and a smaller heliostat area.

To determine the LEC, the cost data of Sargent and Lundy LLC Consulting Group (S&L)(2003) were used as this resulted in a smaller variance when compared to the actual Gemasolar cost. By utilising the results obtained from Figures 26–33, the storage capacity identified for the different exit salt temperatures to obtain the minimum LEC is shown in Table 5. This is with no constraints being placed on the system. It can be noted from the data in Table 5 that the plant has the ability to reach very high capacity factors, which shows that it can perform base load operations.

Table 4 shows that there are two optima of 0.4206 that exist for power block efficiency, one at an exit salt temperature of 290 ˚C and the other at an exit salt temperature of 300 ˚C. Table 5 shows that both configurations result in a minimum LEC scenario. It is recommended that an exit salt temperature of 290 ˚C be selected as this requires a smaller storage facility.

Table 5: Breakdown for optimum storage capacity for different exit salt temperatures

Setup	SM	Exit Salt temp (˚C)	Storage (hours)	Storage mass (tons)	Heliostat area (m^2)	Capital cost (R/W)	CF (%)	LEC S&L (R/k Wh)
1.	2.8	270	16	31 285	1 407 364	86.45	90.38	1.43
2.	2.8	280	16	31 835	1 384 359	85.70	90.32	1.42
3.	3.0	290	16	32 841	1 477 257	87.50	92.19	1.41
4.	3.0	300	16	34 061	1 477 257	87.50	92.16	1.41

Table 6 shows a breakdown of the input cost associated with the optimum plant configurations as shown in Table 5. Figures 34–37 show a breakdown of the costs, and it can be seen that the storage and heliostat field together account for more than 50% of the total cost for the plant.

Table 6: Cost breakdown for optimum storage capacity for different exit salt temperatures for a 100MW_e plant

	Setup 1	Setup 2	Setup 3	Setup 4
Cost breakdown	**$ (million)**	**$ (million)**	**$ (million)**	**$ (million)**
Structures and improvements	16.325	16.058	17.136	17.136
Heliostat field	281.472	276.871	295.451	295.451
Receiver	57.143	57.143	57.143	57.143
Tower piping	16.325	16.058	17.136	17.136

Thermal storage	214.072	187.176	186.427	186.420
Steam generator	3.397	3.342	3.328	3.328
Electric power	55.7	55.7	55.7	55.7
Balance of plant	73.3	73.3	73.3	73.3
Indirect costs	113.4	113.4	113.4	113.4
Contingency	89	89	89	89
Risk pool	64.2	64.2	64.2	64.2
Total cost	$ 984.334	$ 952.248	$ 972.221	$ 972.214

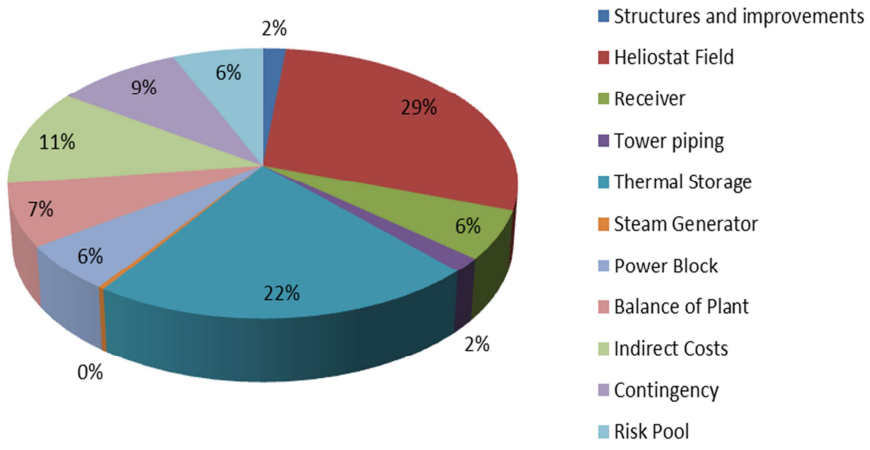

Figure 34: Cost breakdown for exit salt temperature of 270 ˚C, solar multiple of 2.8 and 16 hours thermal energy storage

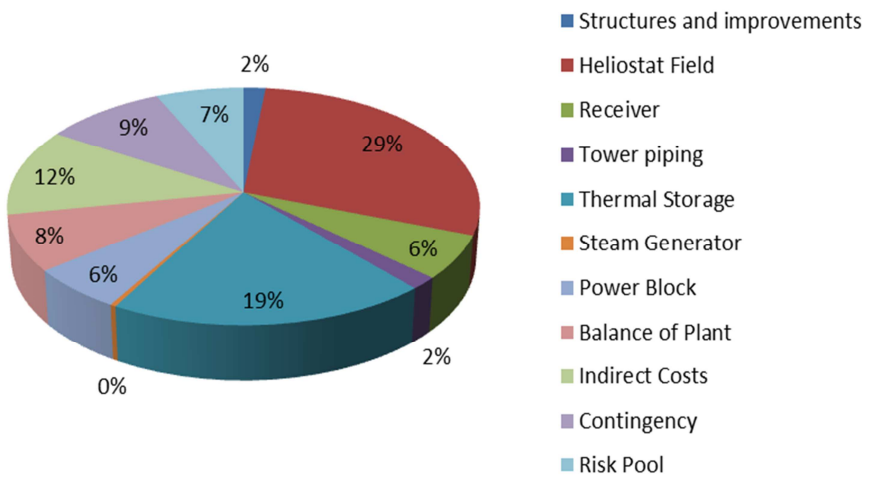

Figure 35: Cost breakdown for exit salt temperature of 280 ˚C, solar multiple of 2.8 and 16 hours thermal energy storage

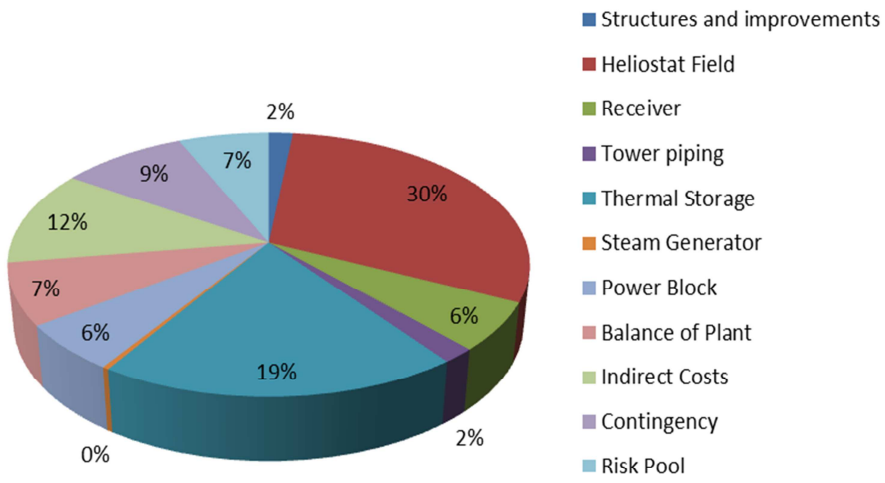

Figure 36: Cost breakdown for exit salt temperature of 290 ˚C, solar multiple 2.8 and 16 hours thermal energy storage

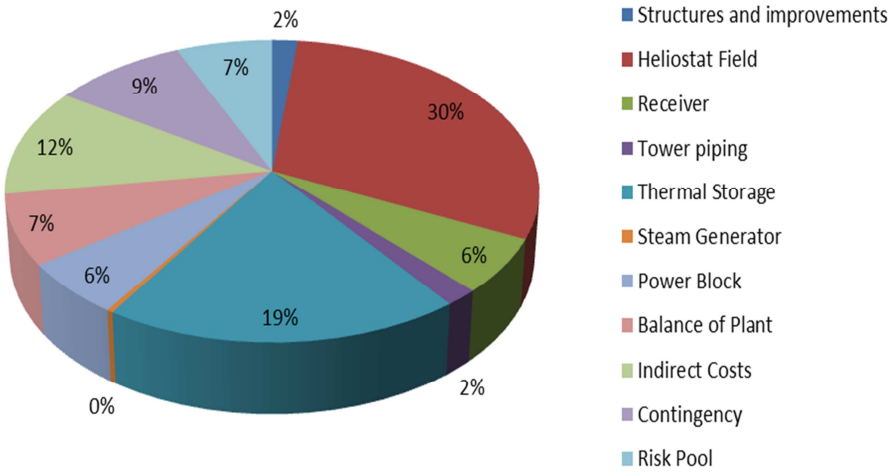

Figure 37: Cost breakdown for exit salt temperature of 300 ˚C, solar multiple of 2.8 and 16 hours thermal energy storage

Consultation with Eskom stakeholders revealed that the proposed plant would have an anticipated 60% capacity factor, and this was used as a constraint to determine the effect on the optimum storage capacity and the plant cost.

For all four exit SG salt temperatures, the lowest LEC with approximately 60% capacity factor (CF) was obtained, with a storage capacity of eight hours and a solar multiple of 1.8, as shown in Table 7. The cost breakdown for the identified configurations is similar and is shown in Figure 38.

Table 7: Breakdown for optimum storage capacity for different exit salt temperatures at 60% capacity factor

SM	**Exit salt temperature (˚C)**	**Storage capacity (hours)**	**S&L cost (R/W)**	**Capacity factor (%)**	**LEC S&L (R/kWh)**
1.8	270	8	67.79	59.10	1.79

1.8	280	8	67.35	58.98	1.78
1.8	290	8	67.24	58.88	1.78
1.8	300	8	67.24	58.82	1.78

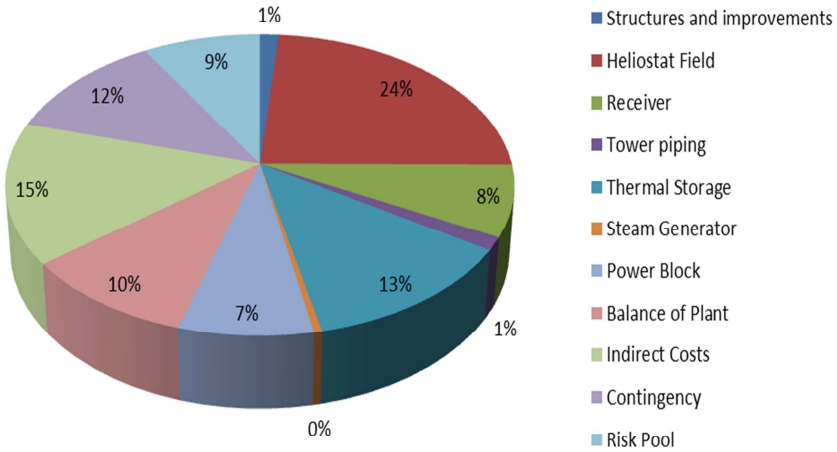

Figure 38: Cost breakdown for 60% capacity factor (solar multiple of 1.8 and eight hours thermal energy storage) (constrained)

A 60% capacity factor results in lower solar multiple and storage capacity and hence lower annual utilisation of the power block. It is thus expected that the resultant LEC would be significantly higher (R1.78) as compared to a storage capacity of 16 hours and a solar multiple of three (R1.41).

8. CONCLUSION

As apparent from the literature survey, the most practical storage medium for commercial electricity production for a central receiver plant was the two-tank molten salt concept as this has made the greatest advancements thus far. It has been proven on a commercial scale with the commissioning of the Gemasolar power plant in Spain. The proposed Eskom plant will be a 100-MW_e central receiver plant with molten salt used as both the HTF and the storage medium. It will be located in the Upington region in South Africa and will feature a dry-cooled power block due to the scarcity of water in the semi-arid conditions.

To determine the power block layout, the exit SG salt temperature was varied between 260 ˚C and 300 ˚C. Varying the power block parameters revealed that an exit salt temperature of 290 ˚C and 300 ˚C, main steam pressure of 140 bar and a final feedwater temperature of 230 ˚C resulted in a power block configuration that resulted in a maximum efficiency of 0.4206 under design point conditions.

Using the identified power block setup and varying the solar multiple and storage capacity indicate that the optimum storage capacity to achieve the lowest LEC for an unconstrained situation is with a solar multiple of three and 16 hours storage. The minimum LEC presents itself for exit salt temperatures of 290 ˚C and 300 ˚C. A higher salt temperature at the SG exit results in an increased mass of salt required in storage. It is recommended that the exit salt temperature be maintained at 290 ˚C. The resultant LEC is R1.41/kWh.

Applying a capacity factor constraint of 60% (as expected in the Eskom demonstration plant), the minimum LEC is achieved with a solar multiple of 1.8 and storage capacity of eight hours. The LEC for this situation is R 1.78/kWh.

The LEC for a supercritical coal plant is R0.80/kWh (International Renewable Energy Agency, 2012a). It is not envisaged that central receiver plants will become cost competitive with coal in the near future due to the infancy of the technology. With the rolling out of the technology on a larger scale and the introduction of carbon taxes CSP could become cost competitive with coal in the longer term.

The high capacity factor presented in the unconstrained case shows that it is possible to utilise this plant for base load power generation.

The capital cost for the unconstrained scenario is R87.50/W and that for the situation with a 60% CF is R67.24/W. There is a major variance in the required capital outlay, and it is concluded that financing limitations placed on the CSP receiver plant of this size would play a major role in determining the CF of the proposed plant.

For both the constrained and unconstrained situations, the majority of the input cost is as a result of the heliostat field and storage. For the unconstrained situation, the heliostat field comprises 30% of the input cost and the storage 19%. In the constrained scenario, the heliostat field makes up 24% and the storage 13% of the input cost.

The model developed provides the basic framework to integrate the components of a central receiver power plant to provide a plant operational model that provides outputs that allow the LEC to be determined. The model can be improved by adding more detail as required.

9. RECOMMENDATIONS

The basic cost framework is provided in the model to calculate the LEC. The data used to determine the input costs are from a 2003 source. The model should be updated with more recent data as these become available, which would result in greater credibility of the plant cost. The power block cost in the model is calculated based on the electrical power output of the plant. It should be updated to allow the power block costs to be calculated in greater detail. This would provide a better understanding of the effect of varying different parameters on the power block (for example, the air-cooled condenser initial temperature difference). The financing parameters surrounding central receiver projects vary, and anyone using the model should insert his or her own best estimates and situation-specific financing data into the model for the LEC calculation.

The model was developed for full-load operation. It is recommended that it be updated to provide the capability to deal with part-load operation.

The value of the power from a demand side tariff structure perspective is not catered for in the model. Currently the lowest LEC based on the storage capacity is determined using an operational strategy that allows the plant to operate at full load. Appendix D shows a proposed demand side tariff structure. This can be incorporated into the model, and the plant can be optimised to determine the ideal operating regime to maximise the profits generated from the plant. This would not yield the same results as when determining the lowest LEC.

The costing data used are based on scenarios and roadmaps created for overseas situations. It should be investigated how the drive by the South African government to localise the industry will influence the costing.

South Africa provides one of the best solar resources in the world, but this is available in sparsely populated areas where the electricity distribution infrastructure is limited. A spinoff from this research could be investigating the extent of infrastructure development required for the Northern Cape region to distribute electricity while preventing total exploitation of the available solar resource.

References

Barlev, D., Vidu, R. & Stroeve, P. 2011. Innovation in concentrated solar power, *Solar energy materials and solar cells*, 95: 2703-2725.

Casals, X.G. 2013. Personal communication, Sunninghill.

Cavallaro, F. 2009. Fuzzy TOPSIS approach for assessing thermal-energy storage in concentrated solar power (CSP) systems, *Applied Energy*, 87: 496-503.

Cengel, Y.A. & Boles, M.A. 2011. *Thermodynamics an engineering approach*. 7th edition. New York. McGraw-Hill

Concentrating solar energy of the future: Torresol Energy's molten salt power tower CSP plant Gemasolar. 2011. [Online]. Available: http://www.solarserver.com/solar-magazine/solar-energy-system-of-the-month/concentrating-solar-energy-of-the-future-torresol-energys-molten-salt-power-tower-csp-plant-gemasolar.html [2013, 9 November].

Concentrating solar power thermal storage system basics. 2013. [Online]. Available: http://energy.gov/eere/energybasics/articles/concentrating-solar-power-thermal-storage-system-basics [2013, 9 November].

Duffie, J.A. & Beckman, W.A. 2006. *Solar engineering of thermal processes*. 3rd edition. New Jersey. John Wiley.

Dunn, R. 2010. *A global review of concentrated solar power storage*, Solar2010, 48th AuSES Annual Conference, 1-3 December 2010, Canberra, Australia.

Fernandes, D., Pitie, F., Caceres, G. & Baeyens, J. 2012. Thermal energy storage: "How previous findings determine current research priorities", *Energy*, 39: 246-257.

Gauche, P., Von Backström, T.W. & Brent, AC. 2011. *CSP modeling methodology for macro decision making – emphasis on the central receiver type*, SolarPACES Conference, Concentrating Solar Power and Chemical Energy Systems, September 20-23, 2011, Granada, Spain.

Gemasolar Thermosolar Plant. s.a. [Online]. Available: http://www.cleanenergyactionproject.com/CleanEnergyActionProject/Energy_Storage_Case_Studies_files/Gemasolar%20Thermosolar%20Plant.pdf [2013, 9 November].

Gemasolar Thermosolar Plant. 2011. [Online]. Available: http://www.nrel.gov/csp/solarpaces/project_detail.cfm/projectID=40 [2013, 9 November].

Gil, A., Martorell, I., Medrano, M., Lazaro, A., Dolado, P., Zalba, B. & Cabeza, L.F. 2009. State of the art on high-temperature thermal energy storage for power generation. Part 1: Concepts, materials and modellization, *Renewable and Sustainable Energy Reviews,* 14: 31-55.

Glatzmaier, G. 2011. Summary Report for Concentrating Solar Power Thermal Storage Workshop. *Technical report, NREL/TP-5500-52134*.

Herrmann, U. & Kearney, D.W. 2002. Survey of thermal energy storage for parabolic trough power plants, *Journal of Solar Energy Engineering,* 124: 145-152.

Ho, C.K., Mahoney, A.R., Ambrosini, A., Bencomo, M., Hall, A. & Lambert, T.N. 2013. Characterisation of Pyromark 2500 paint for high-temperature solar receivers, *Transactions of the ASME,* 136: 014502-1 – 014502-4.

Hoffmann, J.E. 2012. Personal communication, Stellenbosch, hoffmaj@sun.ac.za.

International Energy Agency. 2010. Solar Photovoltaic Energy. *Technology roadmap*.

International Renewable Energy Agency. 2012a. Prospects for renewable power in the South African power pool.

International Renewable Energy Agency. 2012b. Concentrating solar power, *Renewable energy technologies: Cost analysis series*. Volume 1: Power Sector Issue 2/5.

International Renewable Energy Agency. 2012c. Solar photovoltaics, *Renewable energy technologies: Cost analysis series*. Volume 1: Power Sector Issue 4/5.

International Renewable Energy Agency. 2012d. Wind power, *Renewable energy technologies: Cost analysis series*. Volume 1: Power Sector Issue 5/5.

Jones, B. 2012. *Mining the sky* [Online]. Available: http://www.qualitydigest.com/inside/twitter-ed/mining-sky.html [2013, 9 November].

Kearney, D., Kelly, B., Cable, R., Potrovitza, N., Hermann, U., Mahoney, R. & Blake, D. 2002. Assessment of a molten salt heat transfer fluid in a parabolic trough solar field, *Submission to JSEE,*1-20.

Kolb, G.J., Ho, C.K., Mancini, T.R. & Gary, J.A. 2011. Power tower technology roadmap and cost reduction plan, *Sandia Report, Sand 2011-2419*.

Kotze, J.P., Von Backström, T.W. & Erens, P.J. 2013. High-temperature thermal energy storage utilizing metallic phase change materials and metallic heat transfer fluids. *Journal of Solar Engineering,* 135: 35001-1 – 35001-6.

Lata, J.M., Rodriguez, M. & Lara, M.A. 2008. High-flux central receivers of molten salts for the new generation of commercial stand-alone solar power plants. *Journal of Solar Engineering*, 130: 21002-1 – 21002-5.

Liu, M., Saman, W. & Bruno, F. 2012. Review on storage materials and thermal performance enhancement techniques for high-temperature phase change thermal storage systems, *Renewable and Sustainable Energy Reviews*, 16: 2118-2132.

Medrano, M., Gil, A., Martorell, I., Potau, X. & Cabeza, L.F. 2009. State of the art on high-temperature thermal energy storage for power generation. Part 2: Case studies, *Renewable and Sustainable Energy Reviews*, 14: 56-72.

Moran, M.J. & Shapiro, H.N. 2006. *Fundamentals of engineering thermodynamics*. 5th edition. England. John Wiley.

Nag, P.K. 2007. *Power plant engineering*. 3rd edition. New Delhi. McGraw-Hill Education.

Oró, E., Gil, A., De Gracia, A., Boer, D. & Cabeza, L.F. 2012. Comparative life cycle assessment of thermal energy storage systems for solar power plant, *Renewable Energy*, 44: 166-173.

Rajput, R.K. 2007. *Engineering thermodynamics*. 3rd edition, SI units version. New Delhi. Laxmi Publications.

Romero-Paredes, H., Flamant, G., Abanades, S., Charvin, P. & Ambriz, J.J. 2006. *Thermochemical storage of solar energy by means of sulfates: A review*. Proceedings of the 13th SolarPACES Conference, Seville.

Sandia National Laboratories. 2001. Solar power tower, design basis document, Revision 0. *Sand2001-2100.*

Sargent and Lundy LLC Consulting Group. 2003. Assessment of parabolic trough and power tower solar technology cost and performance forecasts. *NREL/SR-550-34440.*

Siemens. 2010. Steam turbines for CSP plants, Industrial Steam Turbines.

Sioshansi, R. & Denholm, P. 2010. The value of concentrating solar power and thermal energy storage. *Technical report, NREL-TP-6A2-45833*.

Solar technology suitability review. 2012. [Online]. Available: http://www.energyandresources.vic.gov.au/energy/sustainable-energy/solar-energy/what/victorias-solar-resources/solar-technology-suitability-review [2013, 9 November].

Steinmann, W.D. & Eck, M. 2006. Buffer storage for direct steam generation. *Solar Energy*, 80:1277–1282.

Tamme, R., Laing, D., Müller-Steinhagen, H. & Steinmann, W.D. 2006. *High-temperature heat storage for industrial process heat and power generation.* Abstract for an oral presentation at the EUROSOLAR Conference.

Thermoflow. 2013. [Online]. Available: http://www.thermoflow.com/convsteamcycle_STP.html [2013, 9 November].

Turchi, C., Mehos, M., Ho, C.K. & Kolb, G.J. 2010. Current and future costs for parabolic trough and power tower systems in the US market, *NREL/CP-5500-49303.*

Tyner, C.E., Sutherland, J.P. & Gould Jr, W.R. Solar Two: A molten salt power tower demonstration. *Sand95-1828C.*

Van Wylen, G.J. & Sonntag, R.E. 1978. *Fundamentals of classical thermodynamics*. SI Version. 2nd revised printing. New York. John Wiley & Sons Inc.

Wikipedia. 2013. *Heliostat.* [Online]. Available: http://en.wikipedia.org/wiki/Heliostat [2013, 12 November].

Wind Energy Centre, University of Massachusetts Amherst. s.a. *Wind power: Capacity factor, intermittency and what happens when the wind doesn't blow* [Online]. Available: http://www.umass.edu/windenergy/publications/published/communityWindFactSheets/RERL_Fact_Sheet_2a_Capacity_Factor.pdf [2013, 9 November].

Appendix A: Planned central receiver plants

Table 8: List of central receiver plants planned or under construction worldwide

Name	Status	Power	Purpose	Country
Crescent Dunes	Under Construction	110 MW	Commercial	USA
Crossroads Solar Energy Project	Planned	150 MW	Commercial	USA
Delingha Supcon Tower Plant	Under Construction	50 MW	Commercial	China
EOS Cyprus	Planned	25 MW	Commercial	Cyprus
Eskom CSP plant	Planned	100 MW	Commercial	South Africa
Gaskell SunTower	Planned	245 MW	Commercial	USA
Ivanpah SEGS	Under Construction	377 MW	Commercial	USA
Khi Solar One	Under Construction	50 MW	Commercial	South Africa
North Midlands Solar Thermal Power Project	Planned	3 MW	Commercial	Australia
Planta Termosolar Maria Elena	Planned	400 MW	Commercial	Chile
Quartzsite	Planned	100 MW	Commercial	USA
Saguache Solar Energy Project	Planned	200 MW	Commercial	USA
Solastor Mejillones	Planned	5 MW	Commercial	Chile
TAQA Concentrated Solar Power Plant	Planned	250 MW	Commercial	Egypt
Termosolar Alcazar	Planned	50 MW	Commercial	Spain

Appendix B: Molten salt data (Sandia National Laboratories, 2001)

Density as a function of temperature:

$$\rho\left(\frac{kg}{m^3}\right) = 2090 - 0.636\,T(℃)$$

Specific heat as a function of temperature

$$c_p\left(\frac{J}{kg℃}\right) = 1443 + 0.172\,T(℃)$$

Absolute Viscosity as a function of temperature:

$$\mu\left(\frac{mPa}{sec}\right) = 22.714 - 0.120\,T + 2.281E-04\,T^2 - 1.474E-07\,T^3$$

Thermal Conductivity as function of temperature

$$k\left(\frac{W}{m℃}\right) = 0.443 + 1.9E-04\,T$$

Appendix C: Sample calculation at design point: 20 March, 12:00

Weather Data for Upington at design point

Month	Day	Hour	Year Day	Year Hour	GHI	DHI	DNI	T_a	$T_{wetbulb}$	Wind Speed
3	20	12	79	1884	882	127	901	29.3	16.4	4.9

Site data

Altitude (m)	814
Longitude (degrees)	21.27
Latitude (degrees)	-28.43
Time zone Longitude (degrees)	30

Assumptions

Heliostat availability	0.99
Heliostat Fouling	0.95
Heliostat Reflectivity	0.95
Heliostat absorptivity	0.9
Receiver emissivity	0.88
Receiver absorbtivity	0.95
Receiver Surface area (m^2)	1000
Receiver Inlet Temperature	Cold Storage Tank Temperature
Receiver Outlet Temperature	Hot Tank Temperature
$T_r = \frac{T_{out}+T_{in}}{2}$	$\frac{565+290}{2} = 427.5\,^{\circ}C$

1. Heliostat field (values are converted to radians for use in Excel)

Convert day of year to angular value:

$$B = \frac{(n_1 - 1)360}{365} \qquad (5.4)$$

$$= \frac{(79 - 1)360}{365}$$

$$= 76.93$$

$$= 1.343\ radians$$

Equation of time:

$$E = 229.2(0.000075 + 0.001868\cos B - 0.032077\sin B - 0.014615\cos 2B - 0.04089\sin 2B) \qquad (5.3)$$

$$= 229.2(0.000075 + 0.001868\cos 1.343 - 0.032077\sin 1.343 - 0.014615\cos 2.686 - 0.04089\sin 2.686)$$

$$= -8.169$$

Solar Time

$$\text{Solar Time} = \text{Standard time} + 4(L_{st} - L_{loc}) + E \qquad (5.2)$$

$$= 12{:}00 + \frac{4(21.27 - 30) - 8.169}{60} - 0.5$$

$$= 10.781$$

Declination

$$\delta = 0.006918 - 0.399912\cos B + 0.070257\sin B - 0.006758\cos 2B + 0.000907\sin 2B - 0.002679\cos 3B + 0.00148\sin 3B \qquad (5.6)$$

$$= 0.006918 - 0.399912\cos 1.343 + 0.070257\sin 1.343 - 0.006758\cos 2.686 + 0.000907\sin 2.686 - 0.002679\cos 4.029 + 0.00148\sin 4.029$$

$$= -0.0079$$

Hour angle

$$\omega = (Solar\ time - 12) * 15 \qquad (5.5)$$

$= (10.781 - 12)(15)$

$= -18.285$

$= -0.319\ radians$

Zenith angle

$\theta_z = \cos^{-1}[\cos\phi\cos\delta\cos\omega + \sin\phi\sin\delta]$ (5.7)

$= cos^{-1}[\cos(-0.496)\cos(-0.0079)\cos(-0.319) + \sin(-0.496)\sin(-0.00794)]$

$= 0.575 radians$

Heliostat field optical efficiency

$Heliostat\ Field\ Optical\ efficiency = 0.4254\theta_z^6 - 1.148\theta_z^5 + 0.3507\theta_z^4 + 0.755\theta_z^3 - 0.5918\theta_z^2 + 0.0816\theta_z + 0.832$ (5.1)

$= (0.4254)(0.575)^6 - (1.148)(0.575)^5 + (0.3507)(0.575)^4 + (0.755)(0.575)^3 - (0.5918)(0.575)^2 + (0.0816)(0.575) + 0.832$

$= 0.808$

2. Receiver

Receiver optical efficiency

$$Receiver\ Opt\ Eff = (Heliostat\ avail\ )(Heliostat\ fouling)(Heliostat\ Refl)(heliostat\ opt\ eff)(1\ -spill) \quad (5.8)$$

$$= (0.99)(0.95)(0.95)(0.808)(1 - 0.15)$$

$$= 0.614$$

Incident energy on receiver

$$Q_{receiver} = (Receiver\ absorbtivity)\ (\ DNI)(Receiver\ opt\ eff)(Field\ aperture)(SM) \quad (5.9)$$

$$= (0.95)\left(901\frac{W}{m^2}\right)(0.614)(497325.50m^2)(1)$$

$$= 2.61\ E08\ W$$

Thermal losses from receiver

Convection loss

$$h = 2.8 + 3(1.5)V \quad (5.11)$$

$$= 2.8 + 3(1.5)\left(4.9\frac{m}{s}\right)$$

$$= 24.85\ \frac{W}{m^2K}$$

$$Q_{conv} = hA(T_r - T_a) \quad (5.12)$$
$$= \left(24.85\frac{W}{m^2K}\right)(1000\ m^2)(427.5\ ^\circ C - 29.3\ ^\circ C)$$
$$= 9.90\ E06\ W$$

Radiation loss

$$Q_{rad} = \varepsilon A\sigma(T_r^4 - T_a^4) \quad (5.13)$$
$$= (0.88)(1000)(5.67E - 08)(700.65^4\ ^\circ K - 302.45^4\ ^\circ K)$$
$$= 1.16\ E07\ W$$

Net energy to salt

$$Q_{net} = Q_{sol} - Q_{conv} - Q_{rad} \quad (5.14)$$
$$= 2.61\ E08\ W - 9.90\ E06\ W - 1.16\ E07\ W$$
$$= 2.40\ E08\ W$$

3. Steam generator pinch point calculation

Total salt flowrate through steam generator:

$$\dot{m}_{SG\ total} = \frac{Q_{SG\ total}}{(C_p)(T_{SG\ in} - T_{SG\ out})}$$

$$where\ Q_{SG\ total} = \left(2975.07\ \frac{kJ}{kg}\right)(\dot{m}_{MS})$$

$$\dot{m}_{SG\ total} = \frac{240177.4011\ \frac{kJ}{s}}{\left(1.51653\frac{kJ}{kg\ ℃}\right)(565\ ℃\ - 290\ ℃)}$$

$$= 575.90\frac{kg}{s}$$

Energy transferred across each component within steam generator:

$$Q_{Preheater} = \left(80.73\frac{kg}{s}\right)\left(1508.899 - 946.99\frac{kJ}{kg}\right)\left(1000\frac{J}{kj}\right) \qquad (5.16)$$

$$= 4.54\ E07\ W$$

$$Q_{Evaporator} = \left(80.73\frac{kg}{s}\right)\left(2668.8 - 1508.899\frac{kJ}{kg}\right)\left(1000\frac{J}{kJ}\right) \qquad (5.16)$$

$$= 9.36\ E07\ W$$

$$Q_{Superheater} = \left(80.73\frac{kg}{s}\right)\left(3471.39 - 2668.8\frac{kJ}{kg}\right)\left(1000\frac{J}{kJ}\right) \qquad (5.16)$$

$$= 6.48\ E07\ W$$

$$Q_{Reheater} = \left(80.73\frac{kg}{s}\right)\left(3567.26 - 3116.58\frac{kJ}{kg}\right)\left(1000\frac{J}{kJ}\right) \qquad (5.16)$$

$$= 3.64\ E07\ W$$

The salt total mass flowrate is configured through the superheater and reheater to allow the exit salt temperature from both components to be equal:

$$\dot{m}_{salt\ superheater} = \frac{\dot{m}_{SG\ total}}{\frac{(Q_{Reheater})(C_p)}{(Q_{Superheater})(C_p)} + 1}$$

$$= \frac{575.90\,\frac{kg}{s}}{\frac{(3.64\ E07\ W)\left(1523.93\,\frac{J}{kg\ ℃}\right)}{(6.48\ E07\ W)\left(1540.2\,\frac{J}{kg\ ℃}\right)} + 1}$$

$$= 370.21\ \frac{kg}{s}$$

$$\dot{m}_{salt\ reheater} = \dot{m}_{SG\ total} - \dot{m}_{salt\ superheater}$$

$$= 575.90\ \frac{kg}{s} - 370.21\ \frac{kg}{s}$$

$$= 205.69\ \frac{kg}{s}$$

Calculation of exit salt temperature from each component

Temperature at exit of superheater and reheater

$$T_{exit\ SH} = T_{salt\ SH\ in} - \left[\frac{Q_{SH}}{(\dot{m}_{SH})(C_p)}\right]$$

$$= 565\ ℃ - \left[\frac{6.48\ E07\ W}{\left(370.21\,\frac{kg}{s}\right)\left(1523.93\,\frac{J}{kg\ ℃}\right)}\right]$$

$$= 450.15\ ℃$$

$$=\ T_{exit\ RH}$$

Temperature at exit of evaporator

$$T_{exit\ Evaporator} = T_{salt\ Evaporator\ in} - \left[\frac{Q_{Evaporator}}{(\dot{m}_{Evaporator})(C_p)}\right]$$

$$= 450.15\ ℃ - \left[\frac{9.36\ E07\ W}{\left(575.90\,\frac{kg}{s}\right)\left(1502.4\,\frac{J}{kg\ ℃}\right)}\right]$$

$= 341.93\ ℃$

Temperature at exit of preheater

$$T_{exit\ preheater} = T_{salt\ preheater\ in} - \left(\frac{Q_{Preheater}}{(\dot{m}_{Preheater})(C_p)}\right)$$

$$= 341.93\ ℃ - \left[\frac{4.54\ E07\ W}{\left(575.90\frac{kg}{s}\right)\left(1502.4\frac{J}{kg\ ℃}\right)}\right]$$

$= 289.50\ ℃$

Pinch point temperature difference

$$Pinch\ Point = T_{salt\ evaporator\ exit} - T_{feedwater\ evaporator\ entrance}$$

$= 341.93\ ℃ - 327.83\ ℃$

$= 14.1\ ℃$

4. Calculation of power block efficiency at design point

The sample calculation for the power block is based on a feedheating system with 5 feedheaters as shown in Figure 39. The parameters at each of the points are obtained using X Steam and are given in Table 8.

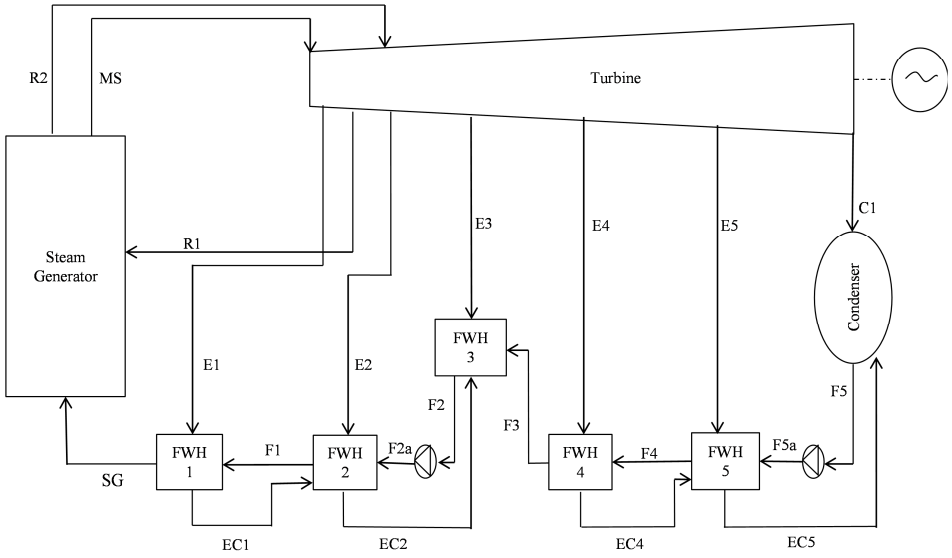

Figure 39: Power block feedwater heating layout with 5 feedwater heaters

Assumptions

- Ambient Temperature = 29.3 ˚C
- Initial Temperature Difference = 20 ˚C
- Condenser Pressure = 0.119 bar
- Main Steam Pressure = 130 bar
- Main Steam Temperature = 550 ˚C
- Reheat Temperature = 550 ˚C
- Equal temperature rise across each feedheater
- $\eta_{turbine}$= 0.85
- Steam Generator feedwater pressure = 135 bar
- Steam Generator feedwater temperature = 220 ˚C
- Gross power output at generator terminals = 100 MW_e
- Pressure at exit of CEX pump is equal to that of open feedwater heater (FWH3)
- Pressure at exit of BFP (F2a) is equal to the steam generator input pressure

Table 9: Properties of feedwater/steam (obtained from X-Steam)

	P (bar)	H (kJ/kg)	T (˚C)	Tsat (˚C)	m (kg/s)	x (steam quality)	S (entropy)
MS	130	3471.39	550		1		6.608
R1	32.5	3116.59	352.56		1	1	6.711
R2	32.5	3567.26	550		1	1	7.338
E1	25.494	3492.35	513.59	225	0.057	1	7.354
E2	12.789	3299.88	418.59	190.86	0.053	1	7.407
E3	5.683	3108.49	321.98	156.72	0.049	1	7.478
E4	2.154	2922.09	225.82	122.58	0.047	1	7.58
E5	0.661	2744.15	132.22	88.44	0.045	1	7.726
C1	0.119	2531.22	49.3		0.749	0.975	7.905
F5	0.119	206.41	49.3		0.842		0.695
F5a	5.683	206.89	49.3		0.842		0.694
F4	5.683	349.80	83.44		0.842		1.116
F3	5.683	493.78	117.58		0.842		1.501
F2	5.683	639.73	151.72		1		1.859
F2a	135	647.74	151.72		1		1.845
F1	135	795.23	185.86		1		2.179
SG	135	946.99	220		1		2.5
EC1	25.494	811.98	190.86		0.057		2.242
EC2	12.789	661.76	156.72		0.109		1.909
EC4	2.154	370.52	88.44		0.048		1.174
EC5	0.661	227.36	54.3		0.093		0.759

Temperature rise across each feedheater:

$$Temperature\ rise = \frac{feedwater\ input\ temp - condenser\ exit\ temp}{number\ of\ feedwater\ heaters} \quad (5.19)$$

$$= \frac{220\ ℃ - 49.3\ ℃}{5}$$

$$= 34.14\ ℃$$

Steam generator

$$\frac{q_{SG,in}}{\dot{m}_{MS}} = (h_{MS} - h_{SG}) \quad (5.20)$$

$$= \left(3471.39 \frac{kJ}{kg} - 946.99\ \frac{kJ}{kg}\right)$$

$$= 2524.4\ \frac{kJ}{kg}$$

$$\frac{q_{RH,in}}{\dot{m}_{MS}} = h_{R2} - h_{R1} \quad (5.21)$$

$$= 3567.26\ \frac{kJ}{kg} - 3116.59\ \frac{kJ}{kg}$$

$$= 450.67\ \frac{kJ}{kg}$$

$$\frac{q_{SG\ total}}{\dot{m}_{MS}} = \frac{q_{SG,in}}{\dot{m}_{MS}} + \frac{q_{RH,in}}{\dot{m}_{MS}}$$

$$= 2524.4\ \frac{kJ}{kg} + 450.67\ \frac{kJ}{kg}$$

$$= 2975.07\ \frac{kJ}{kg}$$

Turbine work

$$\frac{w_{t1}}{\dot{m}_{MS}} = h_{MS} - h_{R1} \quad (5.22)$$

$$= 3471.39\ \frac{kJ}{kg} - 3116.59\ \frac{kJ}{kg}$$

$$= 354.41\ \frac{kJ}{kg}$$

$$where\ h_{R1} = h_{MS} - 0.85(h_{MS} - h_{R1,is})$$

$$\frac{W_{t2}}{\dot{m}_{MS}} = \dot{m}_{E1}(h_{R2} - h_{E1}) + \dot{m}_{E2}(h_{R2} - h_{E2}) + \dot{m}_{E3}(h_{R2} - h_{E3}) + \dot{m}_{E4}(h_{R2} - h_{E4}) + \dot{m}_{E5}(h_{R2} - h_{E5}) + \dot{m}_{C1}(h_{R2} - h_{C1}) \quad (5.23)$$

$$= 0.057\left(3567.26\ \frac{kJ}{kg} - 3492.35\ \frac{kJ}{kg}\right) + 0.053\left(3567.26\ \frac{kJ}{kg} - 3299.88\ \frac{kJ}{kg}\right) + 0.049\left(3567.26\ \frac{kJ}{kg} - 3108.49\ \frac{kJ}{kg}\right) + 0.047\left(3567.26\ \frac{kJ}{kg} - 2922.09\ \frac{kJ}{kg}\right) + 0.045\left(3567.26\ \frac{kJ}{kg} - 2744.15\ \frac{kJ}{kg}\right) + 0.749\left(3567.26\ \frac{kJ}{kg} - 2531.22\ \frac{kJ}{kg}\right)$$

$$= 884.28\ \frac{kJ}{kg}$$

Condenser energy extracted

$$\frac{q_{out,condenser}}{\dot{m}_{MS}} = \dot{m}_{C1}(h_{C1} - h_{F5}) + \dot{m}_{EC5}(h_{EC5} - h_{F5}) \quad (5.24)$$

$$= 0.749\left(2531.22\ \frac{kJ}{kg} - 206.41\ \frac{kJ}{kg}\right) + 0.045\left(227.36\ \frac{kJ}{kg} - 206.41\ \frac{kJ}{kg}\right)$$

$$= 1742.23\ \frac{kJ}{kg}$$

Mass flow rate for extraction points

$$\frac{\dot{m}_{E1}}{\dot{m}_{MS}} = \frac{h_{SG} - h_{F2}}{h_{E1} - h_{EC1}} \quad (5.25)$$

$$= \frac{946.99\ \frac{kJ}{kg} - 795.23\ \frac{kJ}{kg}}{3492.35\ \frac{kJ}{kg} - 811.98\ \frac{kJ}{kg}}$$

$$= 0.0566$$

$$\frac{\dot{m}_{E2}}{\dot{m}_{MS}} = \frac{h_{F2} - h_{F2a} - m_{E1}(h_{EC1} - h_{EC2})}{h_{E2} - h_{EC2}} \quad (5.25)$$

$$= \frac{795.23\ \frac{kJ}{kg} - 647.74\ \frac{kJ}{kg} - (0.0566)\left(811.98\ \frac{kJ}{kg} - 661.76\ \frac{kJ}{kg}\right)}{3299.88\ \frac{kJ}{kg} - 661.76\ \frac{kJ}{kg}}$$

$$= 0.0527$$

$$\frac{\dot{m}_{E3}}{\dot{m}_{MS}} = \frac{h_{16} - (m_{E1} + m_{E2})h_{21} - (1 - m_{E1} - m_{E2})(h_{F3})}{h_{E3} - h_{F3}} \quad (5.25)$$

$$= \frac{639.73\ \frac{kJ}{kg} - (0.0566 + 0.0527)\left(661.76\ \frac{kJ}{kg}\right) - (1 - 0.0566 - 0.0527)\left(493.78\ \frac{kJ}{kg}\right)}{3108.49\ \frac{kJ}{kg} - 493.78\ \frac{kJ}{kg}}$$

$$= 0.0488$$

$$\frac{\dot{m}_{E4}}{\dot{m}_{MS}} = \frac{(1 - m_{E1} - m_{E2} - m_{E3})(h_{F3} - h_{F4})}{h_{E4} - h_{EC4}} \quad (5.25)$$

$$= \frac{(1 - 0.0566 - 0.0527 - 0.0488)\left(493.78\frac{kJ}{kg} - 349.80\frac{kJ}{kg}\right)}{2922.09\ \frac{kJ}{kg} - 370.52\ \frac{kJ}{kg}}$$

$$= 0.0475$$

$$\frac{\dot{m}_{E4}}{\dot{m}_{MS}} = \frac{(1 - m_{E1} - m_{E2} - m_{E3})(h_{F4} - h_{F5}) + m_{E4}(h_{EC5} - h_{EC4})}{(h_{E5} - h_{EC5})} \quad (5.25)$$

$$= \frac{(1 - 0.0566 - 0.0527 - 0.0488)(349.80\ - 206.41\ )\frac{kJ}{kg} + (0.0475)(227.36\ - 370.52\ )\frac{kJ}{kg}}{2744.15\ \frac{kJ}{kg} - 227.36\ \frac{kJ}{kg}}$$

$$= 0.0453$$

Pump work

$$\frac{w_{p1}}{\dot{m}_{MS}} = \dot{m}_{F5}(h_{F5a} - h_{F5}) \quad (5.26)$$

$$= (0.842)\left(206.89\,\frac{kJ}{kg} - 206.41\,\frac{kJ}{kg}\right)$$

$$= 0.4047\,\frac{kJ}{kg}$$

$$\frac{w_{p2}}{\dot{m}_{MS}} = (h_{F2a} - h_{F2}) \tag{5.27}$$

$$= \left(647.74\ \frac{kJ}{kg} - 639.73\ \frac{kJ}{kg}\right)$$

$$= 8.01\ \frac{kJ}{kg}$$

Gross thermal efficiency

$$\eta_{thermal} = \frac{w_{t1}+w_{t2}}{q_{SG\ total}} \tag{5.28}$$

$$= \frac{354.4\,1\,\frac{kJ}{kg} + 884.28\ \frac{kJ}{kg}}{2975.07\ \frac{kJ}{kg}}$$

$$= 0.4163$$

Mass flow rate for steam

$$\dot{m}_{MS} = \frac{(100)(1000)}{w_{t1}+w_{t2}} \tag{5.29}$$

$$= \frac{100000\ kW}{354.41\ \frac{kJ}{kg} + 884.28\ \frac{kJ}{kg}}$$

$$= 80.73\,\frac{kg}{s}$$

5. Number of heliostats for SM =1 at design point

$\eta_{power\ block\ DP} = 0.4163$

Storage required for 1 hour operation (energy)

$$\frac{Energy\ Stored}{3\,600\ s} = \frac{Gross\ Power\ Output}{Reference\ Power\ Block\ Efficiency_{1\ hour}} \quad (5.15)$$

$$= \frac{1\ \ E08\ W}{0.4163}$$

$$= 2.40\ E08\ W$$

Energy required from solar field

$$Energy\ from\ Solar\ Field = \frac{Storage_{1\ hour}}{(Ref\ Receiver\ Opt\ Eff)(Reference\ receiver\ thermal\ eff)(Receiver\ absorbtivity)} \quad (5.29a)$$

$$= \frac{2.40\ E08\ W}{(0.614)(0.919)(0.95)}$$

$$= 4.48\ E8\ W$$

Aperture area

$$Field\ Aperture = \frac{Energy\ from\ Solar\ Field}{Reference\ DNI} \quad (5.30)$$

$$= \frac{4.48\ E08\ W}{901\ \frac{W}{m^2}}$$

$$= 497325.50\ m^2$$

Number of heliostats

$$Number\ of\ Heliostats = \frac{Aperture\ area}{heliostat\ size} \quad (5.31)$$

$$= \frac{497325.50\ m^2}{120\ m^2}$$

$$= 4144\ heliostats$$

6. Sample LEC calculation

A sample LEC calculation will be performed for a solar multiple of 2 with 8 hours of storage. The calculation will be based on values extracted from the plant model developed.

Parameter	Model output
Aperture Area (m^2)	994048
Receiver Surface Area (m^2)	1000
Thermal Storage Capacity (kW_t)	1.9 E06
Steam Generator Capacity (kW_t)	240000
Gross Electric Power (kW_e)	100000

The cost categories multiplied by their respective parameters and are shown in dollars

Cost Category	**Sunlab**	**Sargent and Lundy**
Structures and improvements ($)	12226790	11530957
Heliostat Field ($)	198809600	198809600
Receiver ($)	50000000	57143000
Tower and piping ($)	12027981	11530957
Thermal Storage ($)	94082076	94082076
Steam Generator ($)	3360074	3360074
Electric Power ($)	73050000	55700000
Balance of Plant ($)	53200000	73300000
Indirect Costs ($)	44000000	113400000
Contingency ($)	45300000	89000000

Risk Pool ($)	58000000	64200000
Total Plant Cost ($)	644056522	772056664
Operation and Maintenance ($)	6500000	6500000

LEC calculation for Sargent Lundy cost

Year	Loan Balance (R)	O&M (R)	Annual cost[1]	$\sum_{t=1}^{n} \frac{I_t + M_t + F_t}{(1+r)^t}$	Energy produced (kWhr)	$\sum_{t=1}^{n} \frac{E_t}{(1+r)^t}$	Cost R/kWh
1	6948509977	58500000	824003948.8	780306769.7	552700000	5.23E+08	1.71
2	6877857026	64350000	829853948.8	744172862.1	552700000	4.96E+08	
3	6800138780	70785000	836288948.8	710173729.8	552700000	4.69E+08	
4	6714648709	77863500	843367448.8	678205272.7	552700000	4.44E+08	
5	6620609631	85649850	851153798.8	648169290.5	552700000	4.21E+08	
6	6517166646	94214835	859718783.8	619973185.8	552700000	3.99E+08	
7	6403379361	103636319	869140267.3	593529683.7	552700000	3.77E+08	
8	6278213349	113999950	879503899.1	568756566.2	552700000	3.57E+08	
9	6140530735	125399945	890903894.2	545576422.2	552700000	3.38E+08	
10	5989079860	137939940	903443888.7	523916411.1	552700000	3.21E+08	
11	5822483897	151733934	917237882.7	503708040	552700000	3.04E+08	
12	5639228338	166907327	932411276.1	484886953.1	552700000	2.87E+08	
13	5437647223	183598060	949102008.8	467392733.3	552700000	2.72E+08	
14	5215907996	201957866	967461814.8	451168715.8	552700000	2.58E+08	
15	4971994847	222153653	987657601.4	436161811.2	552700000	2.44E+08	
16	4703690383	244369018	1009872967	422322340.2	552700000	2.31E+08	
17	4408555472	268805920	1034309868	409603877.3	552700000	2.19E+08	
18	4083907071	295686512	1061190460	397963104.1	552700000	2.07E+08	
19	3726793829	325255163	1090759112	387359671.5	552700000	1.96E+08	
20	3333969263	357780679	1123284628	377756070.1	552700000	1.86E+08	
21	2901862241	393558747	1159062696	369117508.9	552700000	1.76E+08	
22	2426544516	432914622	1198418571	361411801.5	552700000	1.67E+08	
23	1903695019	476206084	1241710033	354609259.4	552700000	1.58E+08	

24	1328560572	523826692	1289330641	348682593.1	552700000	1.49E+08	
25	695912681	576209362	1341713310	343606818.4	552700000	1.42E+08	
Total				1.25E+10		7.34E+09	

[1]The annual cost is the sum of the loan outstanding and the operation and maintenance cost.

Appendix D: Time of use tariffs

Table 10 : CSP time of use tariffs (ARUP memorandum, 2013)

	Time of day for energy delivery	Effective price cap
Standard time	Every day 5:00am - 04:59pm 9:00pm – 9:59pm	R 1650/MWh
Peak Time	Every day 5:00pm – 8:59pm	R 3960/MWh
Night time	Everyday 10:00pm – 4:59pm	R0/MWh